Journal of Nanobiotechnology

RESEARCH Open Access

Intranasal delivery of engineered extracellular vesicles promotes neurofunctional recovery in traumatic brain injury

Pengtao Li[1†], Sishuai Sun[1†], Xingyu Zhu[2], Xiaoyu Liu[1], Rui Yin[1], Yihao Chen[1], Jianbo Chang[1], Liguo Ye[1], Jingxi Gao[2], Xiaoyan Zhao[2], Houshi Xu[1], Yue Wang[1], Wei Zuo[1], Zhao Sun[3], Shihua Wang[2], Xiao Zhang[1], Junji Wei[1*], Robert Chunhua Zhao[2*] and Qin Han[2*]

Abstract

Traumatic brain injury (TBI) is a leading cause of disability in adults, significantly affecting patients' quality of life. Extracellular vesicles (EVs) derived from human adipose-derived mesenchymal stem cells (hADSCs) have demonstrated therapeutic potential in TBI treatment. However, their limited targeting ability, short half-life, and low bioavailability present significant challenges for clinical application. In this study, we engineered extracellular vesicles (EEVs) by transfecting hADSCs with lentivirus and incorporating ultra-small paramagnetic nanoparticles (USPNs), resulting in EVs with enhanced miRNA expression and targeted delivery capabilities. These EEVs were administered intranasally to specifically target injury sites, effectively modulating the NF-κB signaling pathway to suppress neuroinflammation. In both in vitro and in vivo assessments, EEVs exhibited superior efficacy in promoting neurofunctional recovery and neurogenesis after brain injury compared to unmodified EVs. Furthermore, validation using human brain organoid models confirmed EEVs' remarkable ability to suppress neuroinflammation, offering a promising strategy for TBI treatment.

Introduction

Traumatic brain injury (TBI) refers to structural or functional changes in the brain, accompanied by temporary or permanent neurological dysfunction, caused by brain tissue damage following blunt force or penetrating injuries to the head. It remains a significant public health challenge, especially in developing countries [1, 2]. Despite prompt medical intervention, severe TBI often leads to serious and permanent disabilities [3]. The pathophysiology of TBI involves the disruption of cellular barriers and the persistent release of inflammatory factors, which subsequently cause neuronal apoptosis, necrosis, and fibrosis. Excessive inflammatory responses, driven by pro-inflammatory cytokines such as interleukin-1 (IL-1) and tumor necrosis factor-α (TNF-α), directly mediate neuroinflammatory damage by activating inflammatory signaling pathways, thereby exacerbating secondary central nervous system (CNS) injury [4, 5]. Timely neutralization of these inflammatory mediators, inhibition of immune cell recruitment, minimization of tissue damage, and promotion of tissue repair and regeneration are critical strategies. However, to date,

†Pengtao Li and Sishuai Sun are co-first authors.

*Correspondence:
Junji Wei
weijunji@pumch.cn
Robert Chunhua Zhao
zhaochunhua@ibms.pumc.edu.cn
Qin Han
hangin@ibms.pumc.edu.cn

Full list of author information is available at the end of the article

Graphical abstract

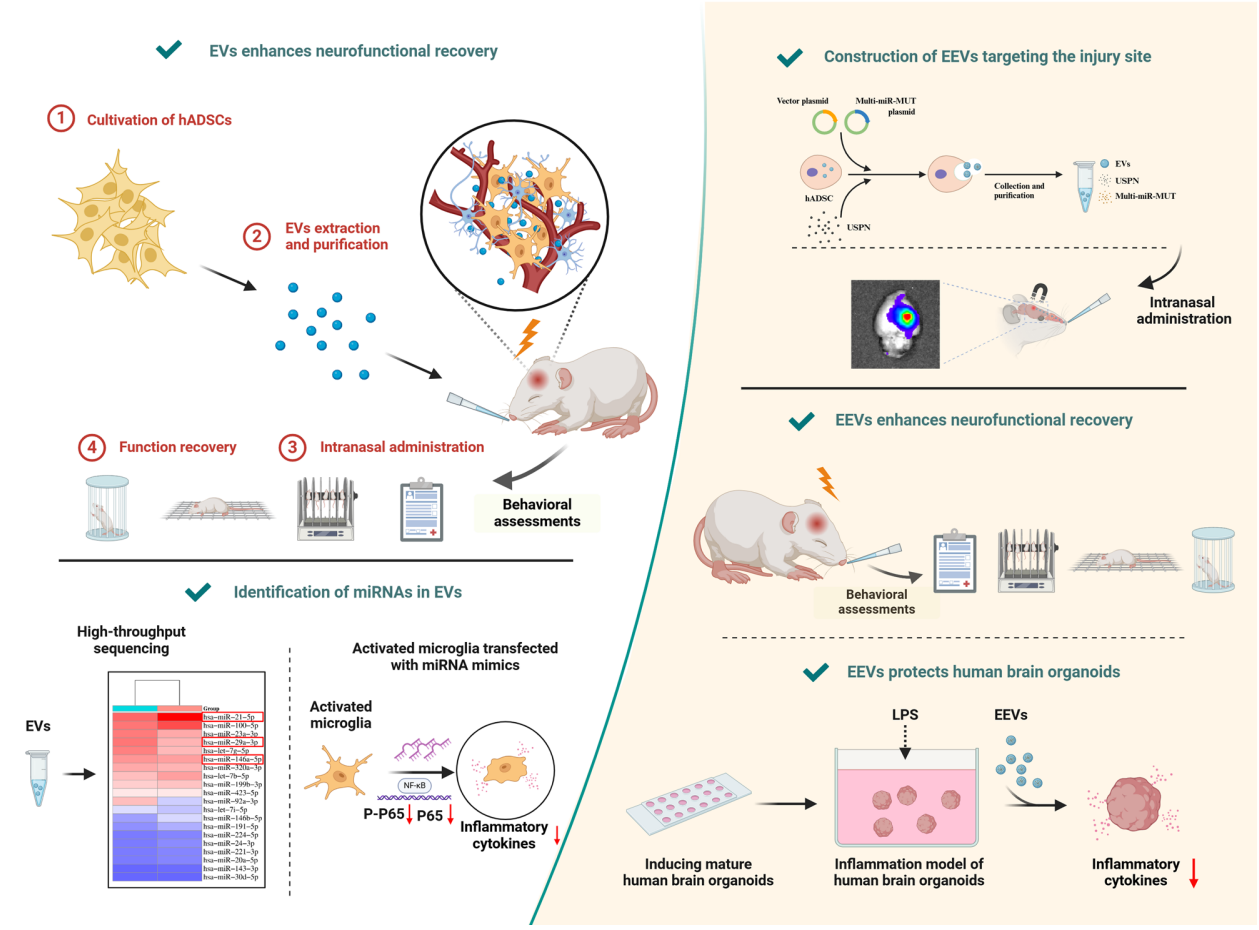

Keywords Traumatic brain injury, Engineered extracellular vesicles, NF-κB, Neuroinflammation, Neurofunctional recovery

no drug specifically targeting TBI has been approved by the U.S. Food and Drug Administration (FDA) [6]. Thus, developing strategies to enhance brain injury recovery and improve long-term functional outcomes remains an urgent research priority with the potential to benefit a large number of patients.

Human adipose-derived stem cells (hADSCs) are ideal candidates for regenerative medicine due to their multipotency, angiogenic, anti-apoptotic, and immunomodulatory properties [7, 8]. Preclinical studies and clinical trials have demonstrated the therapeutic potential of hADSCs in various applications, including fat grafting [9], wound healing [10], bone regeneration [11], skeletal muscle repair [12], cardiac repair [13], and nerve regeneration [14]. A key advantage of hADSCs is their accessibility via minimally invasive procedures, enabling the collection of large cell quantities [8]. However, clinical translation of stem cell therapies faces challenges, including ethical issues, maintaining cell viability, and risks like immunogenicity, tumorigenicity, or inappropriate differentiation. Recent research suggests that the therapeutic effects of hADSCs are mediated primarily through the extracellular vesicles (EVs) they secrete [15].

EVs are small membrane vesicles (20–1000 nm) of endosomal origin secreted by cells via exocytosis. These vesicles contain proteins, lipids, metabolites, and nucleic acids that are associated with specific cellular functions [16]. Notably, EVs have lower immunogenicity than cells, enabling them to bypass biological barriers and evade immune clearance [17]. This makes EVs promising natural nanocarriers for drug delivery. EVs derived from hADSCs have shown potential in mitigating injury and promoting regeneration in tissues such as skin, nerves, and cartilage [8]. Our previous studies showed that intraventricular injection of hADSC-derived EVs significantly reduces neuroinflammation and promotes neurogenesis

after TBI [18]. However, research on the applications of EVs in TBI remains limited, likely due to challenges such as poor targeting ability, short half-life, low bioavailability, and reliance on invasive delivery methods [19, 20].

Advances in bioengineering have significantly enhanced the stability, circulation half-life, and targeting capabilities of EVs, thereby improving their bioavailability and therapeutic outcomes. For example, pretreatment of mesenchymal stem cells (MSCs) with brain-derived neurotrophic factor (BDNF) has been shown to produce BDNF-modified MSC-derived EVs with superior anti-inflammatory and neuroregenerative effects compared to unmodified EVs [21]. Zhang et al. EVs enriched with microRNA-210 were shown to enhance vascular endothelial growth factor (VEGF) expression and improve angiogenesis [22]. Additionally, engineering modifications can increase EVs cargo capacity and targeting specificity. For instance, Tian et al. conjugated the c(RGDyK) peptide to the EVs surface, enabling intravenous cRGD-EVs to specifically target ischemic brain injury regions [23]. Similarly, Alvarez et al. engineered dendritic cells to express Lamp2b, an exosomal membrane protein fused with neuron-specific RVG peptides, enhancing the targeting of EVs to neurons [24]. Furthermore, our team's meta-analysis of preclinical studies on ischemic stroke treatment revealed that engineered extracellular vesicles (EEVs) demonstrated superior therapeutic efficacy compared to natural EVs [25].

One of the significant challenges in the application of EVs in the CNS is the restriction imposed by the blood-brain barrier (BBB), which significantly limits the bioavailability of systemically administered EVs. Although intraventricular and intrathecal administration can bypass the BBB, these methods carry risks of hemorrhage and infection with repeated use, making them less favorable [26, 27]. Recently, intranasal administration has emerged as a promising, non-invasive alternative for drug delivery to the brain, as it can circumvent the BBB [28]. Studies have shown that MSC-derived EVs can directly reach the brain following intranasal delivery [29, 30]. Notably, MSC-derived EVs exhibit strong migration and homing abilities, particularly targeting neurons [31]. This migration and homing capability is significantly influenced by inflammation, which plays a key role in these mechanisms [31]. Additionally, EVs can fuse directly with cell membranes via CD9 tetraspanins, bypassing endosomal capture [32]. This characteristic ensures direct cytosolic delivery of exosomal cargo, avoiding the barriers associated with endosomal sequestration. Therefore, intranasal administration is considered a viable option for brain drug delivery, offering substantial potential for clinical application [33].

In this study, we first demonstrated that continuous intranasal administration of EVs significantly improved neurological function in TBI rats. We found that EVs exert their effects by inhibiting NF-κB signaling, thereby reducing microglial activation. High-throughput miRNA sequencing of EVs identified candidate miRNAs that potentially target the NF-κB pathway and suppress neuroinflammation. Subsequently, we successfully EEVs loaded with these candidate miRNAs and ultrasmall superparamagnetic nanoparticles (USPN) for targeted delivery to the injury site. The experimental characterization results showed that EEVs achieved efficient utilization in both rat and human brain organoid models, demonstrating superior therapeutic efficacy (Graphical Abstract).

Results

Continuous intranasal administration of EVs improves neurological function in TBI rats

Our laboratory has been extensively studying the role of EVs in brain injury for over a decade. In this study, EVs were successfully extracted and characterized (Figure S1A-C). We investigated the potential of continuous intranasal administration of EVs to improve neurological function in TBI rats. A TBI model was established in male Sprague-Dawley (SD) rats that were pre-trained to perform neurological and behavioral tasks prior to surgery. This was followed by intranasal administration of PBS, hADSC, or EVs 24 h post-surgery, once weekly for 28 days (Fig. 1A). Neurological and motor functions were assessed on days 1, 4, 7, 14, 21, and 28 post-treatment using the modified neurological severity score (mNSS), Foot-Fault Test, Rotarod Test, and Cylinder Test. As shown in Fig. 1B, the mNSS assessment revealed that rats treated with EVs exhibited significant improvements in neurological function compared to the PBS-treated group by day 28. The Foot-Fault Test (Fig. 1C) demonstrated a reduction in forelimb slips in the EVs-treated group compared to the PBS-treated group, with significant differences observed starting at day 4. Similarly, in the Rotarod Test (Fig. 1D), EVs-treated group displayed a significantly longer latency to fall compared to the PBS-treated group from day 4 onwards. The Cylinder Test (Fig. 1E) revealed a substantial reduction in forelimb use asymmetry score in the EVs-treated group compared to PBS-treated group, starting from day 4. Collectively, these results indicate that EVs therapy significantly promotes neurological recovery following TBI.

EVs reduce microglial activation by inhibiting the NF-κB signaling pathway

To elucidate the mechanisms underlying the neuroprotective effects of EVs in TBI rats, we investigated their impact on microglial activation. As shown in Fig. 2A, intranasally administered PKH67-labeled EVs were primarily taken up by microglia (IBA1) and neurons (NeuN).

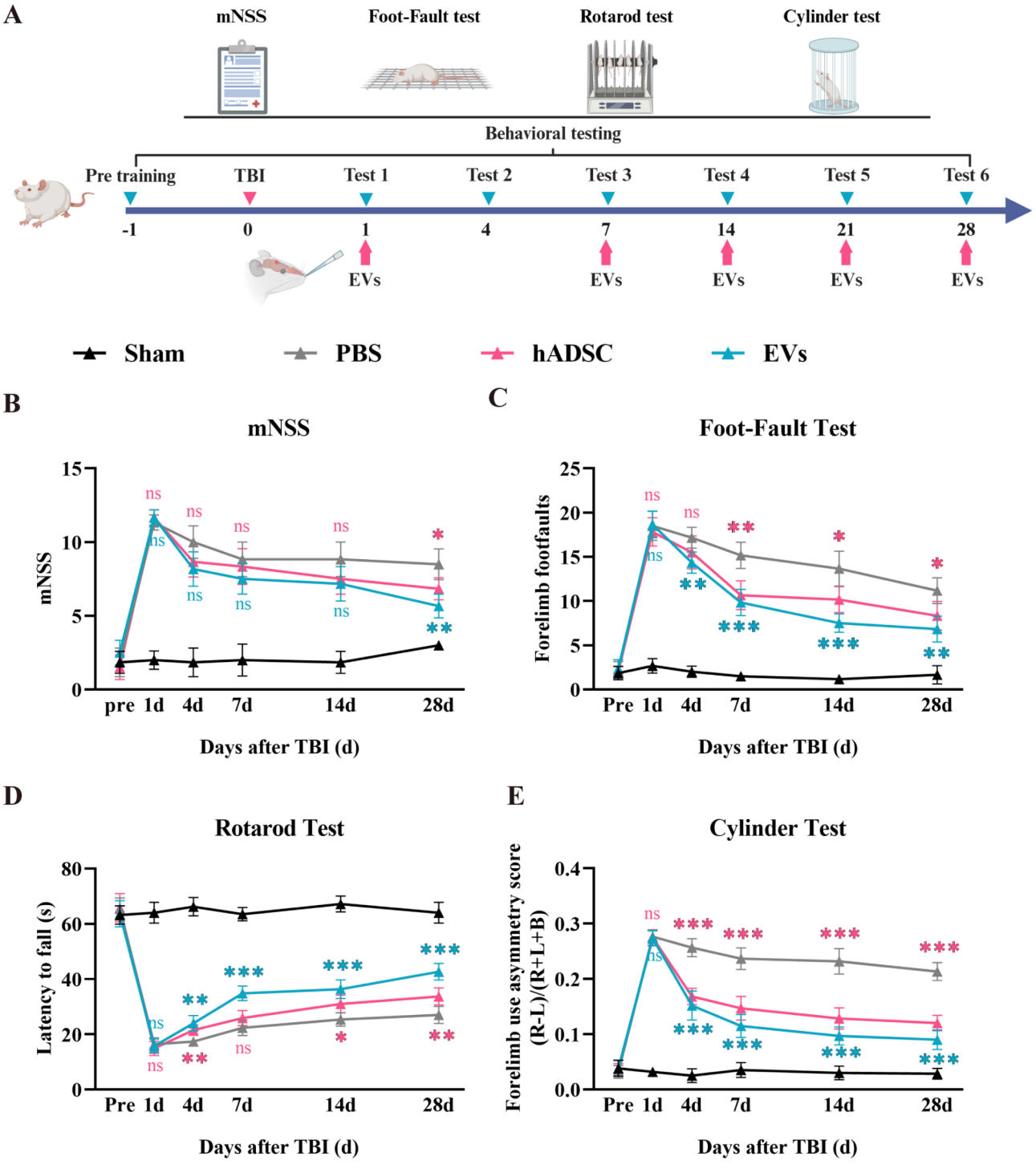

Fig. 1 Intranasal administration of EVs enhances neurofunctional recovery in TBI rats. (**A**) Schematic representation of the experimental timeline for EVs administration and subsequent behavioral assessments. Neurological and motor function recovery at various time points post-injury were evaluated using mNSS (**B**), Foot-Fault Test (**C**), Rotarod Test (**D**), and Cylinder Test (**E**) ($n=6$). Statistical analysis was performed using two-way repeated measures ANOVA followed by the Holm-Sidak post hoc multiple comparison test. Color Coding and Statistical Comparisons: Red (hADSC): hADSC-treated group compared to PBS. Blue (EVs): EVs-treated group compared to PBS. *$P<0.05$, **$P<0.01$, ***$P<0.001$. mNSS: Modified Neurological Severity Score

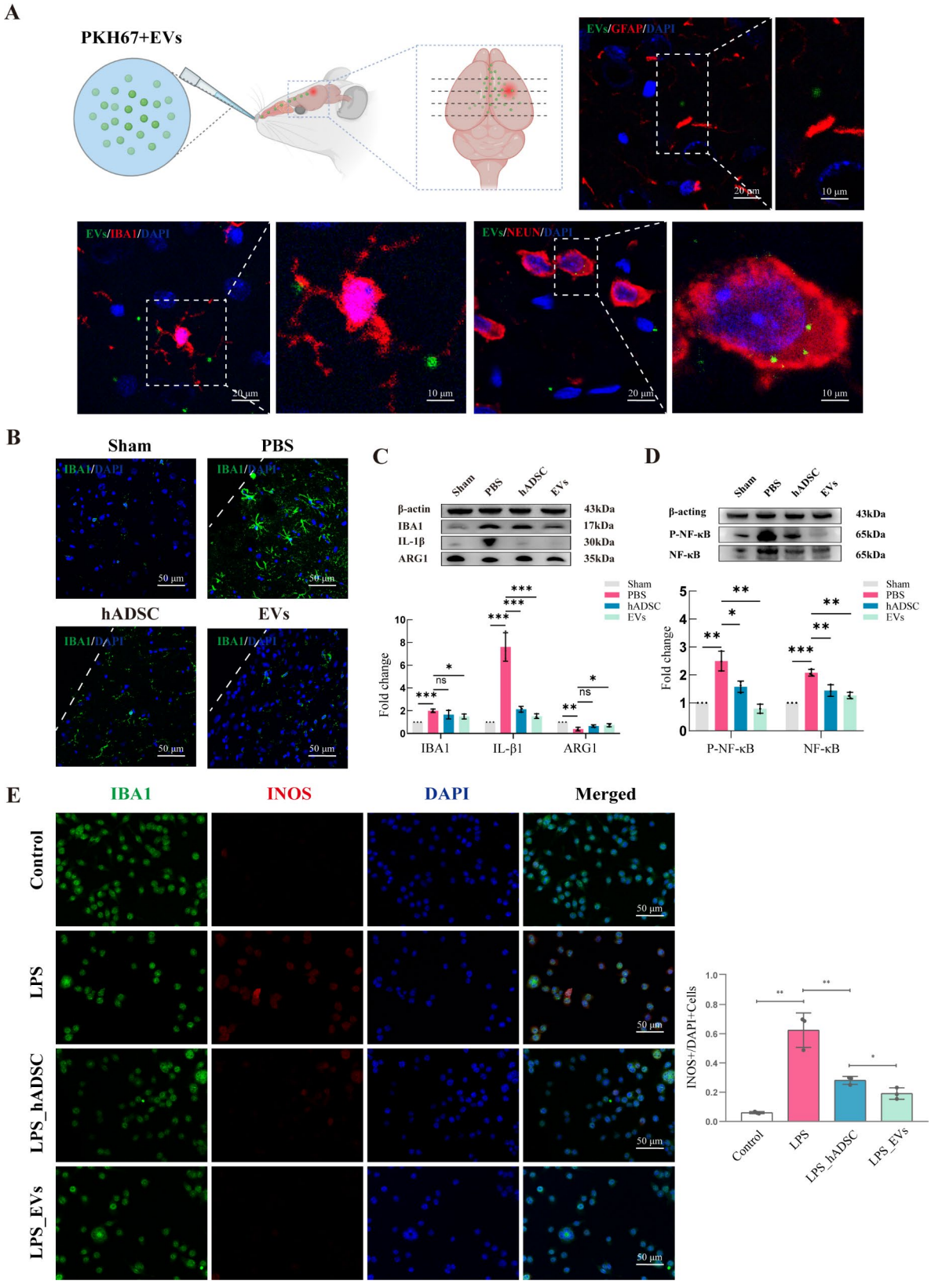

Fig. 2 (See legend on next page.)

(See figure on previous page.)

Fig. 2 EVs inhibit microglial activation by suppressing the NF-κB signaling pathway. (**A**) Immunofluorescence (IF) showing the distribution of EVs (PKH67-labeled EVs) in neurons (NeuN), astrocytes (GFAP), and microglia (IBA1) 48 h post-intranasal administration in TBI rats. (**B**) IF of IBA1 in the perilesional cortex 5 days post-TBI under different treatment conditions. (**C**) Western blot analysis showing the expression of IBA1, INOS, IL-1β, and ARG1 in the perilesional cortex on day 5 post-injury ($n=3$). (**D**) Western blot analysis of NF-κB signaling pathway proteins (P-NF-κB and NF-κB) in the perilesional cortex on day 5 post-injury ($n=3$). (**E**) IF of IBA1 (green) and INOS (red) in an in vitro BV2 microglial activation model treated with 5.0×10^5 hADSCs or 20 μg total protein of EVs ($n=3$). $^*P<0.05$, $^{**}P<0.01$, $^{***}P<0.001$. NeuN: Neuron-specific nuclear protein; GFAP: Glial Fibrillary Acidic Protein; IBA1: Ionized Calcium-Binding Adapter Molecule 1; IL-1β: Interleukin-1 beta; INOS: Inducible Nitric Oxide Synthase; ARG1: Arginase 1; LPS: Lipopolysaccharide

This immunofluorescence (IF) analysis is qualitative and highlights the localization of EVs in the peri-lesional cortex, indicating preferential uptake by microglia and neurons. Additionally, we included a control brain from the PKH67 dye-only treated group, which was imaged under the same conditions without EVs (Supplementary Figure S2A).

Compared to the PBS and hADSC groups, EVs treatment significantly suppressed microglial activation in the peri-lesional cortex 5 days post-injury (Fig. 2B). Western blot analysis showed that EVs treatment significantly reduced the expression of IBA, inducible nitric oxide synthase (INOS)，and IL-1β in the peri-lesional cortex of TBI rats, while also increasing the expression of Arginase 1 (ARG1) (Fig. 2C).

The NF-κB signaling pathway is a critical regulator of microglial activation and inflammation in CNS [34–36]. To determine whether EVs reduce microglial activation via the NF-κB pathway, we assessed the activation of NF-κB signaling pathway proteins (P-NF-κB and NF-κB) in the peri-lesional cortex of TBI rats at 28 days post-injury. As depicted in Fig. 2D, EVs treatment significantly lowered the expression levels of both P-NF-κB and NF-κB proteins, suggesting that EVs modulate microglial activation through NF-κB signaling inhibition. Additionally, in an in vitro model of lipopolysaccharide (LPS)-induced activation of BV2 microglial cells, IF demonstrated that EVs treatment markedly reduced INOS expression compared to the control and hADSC groups (Fig. 2E). In this experiment, hADSCs were co-cultured with LPS-induced BV2 microglial cells using a Transwell system, which allowed the exchange of soluble factors without direct cell-cell contact. Moreover, in an in vitro model of LPS-induced BV2 microglial activation, qRT-PCR analysis demonstrated that EVs treatment significantly reduced the expression levels of inflammatory factors (IL-1α, IL-1β, IL-6, CCL3, INOS, TNF-α) compared to the control and hADSC groups (Supplementary Figure S2A). IF results further confirmed that EVs treatment markedly reduced the expression of INOS (Fig. 2E) and increased the expression level of ARG1 (Supplementary Figure S2B).

Identification of miRNAs in EVs that target the NF-κB pathway to inhibit microglial activation

Recent studies have demonstrated that microRNAs (miRNAs), key regulators of gene expression, play a crucial role in the therapeutic effects of EVs [37]. We performed high-throughput miRNA sequencing on EVs derived from hADSCs (two healthy donors) to identify miRNAs associated with the NF-κB signaling pathway and microglial activation. This analysis revealed 20 miRNAs that were consistently upregulated across samples (Fig. 3A).

We transfected BV2 microglial cells with miRNA mimics and used qRT-PCR to assess their effects on inflammatory cytokine expression in a microglial activation model. The results showed that hsa-miR-21-5p, hsa-miR-29a-3p, and hsa-miR-146a-5p effectively inhibited microglial activation, with the combination of all three miRNAs significantly reducing the expression of pro-inflammatory cytokines (Fig. 3B). IF analysis further validated these findings, revealing that co-transfection with the three miRNAs significantly suppressed INOS expression (Fig. 3C) while enhancing ARG1 expression, indicating a shift towards an anti-inflammatory phenotype (Supplementary Figure S3A). Western blot analysis further demonstrated that transfection with these three miRNAs inhibited the NF-κB signaling pathway by reducing the expression of P-NF-κB and NF-κB proteins (Fig. 3D).

Construction of EEVs targeting the injury site

To explore the role of these three miRNAs in the pathological process of TBI, we constructed engineered extracellular vesicles (EEVs) designed to specifically target the injury site. As illustrated in Fig. 4A, we first developed a lentiviral vector that overexpresses the three miRNAs, designated as Multi-miR-MUT. This lentiviral construct was used to transfect hADSCs. To enhance the targeting capability of EEVs, ultra-small paramagnetic nanoparticles (USPN) were added to the hADSC culture medium. The transfected cells then secreted EEVs enriched with the three miRNAs and loaded with USPN, which were subsequently isolated and purified through ultrafiltration. Fluorescence microscopy confirmed that the transfected hADSCs exhibited strong green fluorescence (Fig. 4B). qRT-PCR results indicated that the expression levels of the three miRNAs in the transfected hADSCs were significantly higher than those in the control group (Fig. 4C), confirming the successful construction of engineered hADSCs expressing high levels of the target miRNAs.

To evaluate the cytotoxicity of USPN on hADSCs, various concentrations of USPN (5, 10, 20, 40, 80, 160, 320 μg/mL) were added to the hADSC culture medium. The Cell Counting Kit-8 (CCK8) assay results indicated a significant decrease in cell viability at a concentration of 320 μg/mL (Fig. 4D). We then introduced different concentrations of USPN (80 μg/mL and 160 μg/mL) and examined intracellular vesicle morphology using transmission electron microscopy (TEM), observing significant accumulation of USPN in vesicles at 160 μg/mL (Fig. 4E). This finding was further corroborated by Prussian blue staining (Supplementary Figure S4A). Nanoparticle tracking analysis (NTA) demonstrated that EEVs had a size distribution centered around 118 nm (Fig. 4F). Western blot analysis confirmed the presence of classical extracellular vesicle markers, including ALIX, HSP90, and CD63, in the EEVs (Fig. 4G). Further TEM analysis provided additional confirmation of the extracellular vesicle structure (Fig. 4H). qRT-PCR results revealed high expression levels of the three miRNAs in the EEVs (Fig. 4I).

To assess the targeting ability of EEVs, we pre-labeled EVs and EEVs with Dil dye and administered EEVs intranasally 24 h after TBI induction in rats. In vivo imaging conducted 48 h post-administration revealed that EEVs, subjected to external magnetic targeting, effectively targeted the injury site compared to the EVs group (Fig. 4J). Subsequently, we found that after intranasal administration, EVs and EEVs primarily concentrated in the brain and lungs (Supplementary Figure S4B). Brain tissue slices from the rats were analyzed, and IF showed that EEVs significantly accumulated in the perilesional area compared to the EVs and PBS groups (Fig. 4K). Prussian blue staining of brain tissue slices post-treatment further confirmed that EEVs successfully localized to the perilesional area (Supplementary Figure S4C). Additionally, qRT-PCR analysis revealed significantly elevated levels of the three miRNAs in the brain and lungs compared to the control group (Supplementary Figure S4D-F). These results demonstrate that EEVs exhibit strong targeting capability and effectively localize to the TBI injury site.

EEVs promote neurofunctional recovery in TBI rats

We next assessed the impact of EEVs on neurofunctional recovery in a TBI rat model. Following established protocols, PBS, EVs, or EEVs were administered intranasally 24 h after TBI induction, with treatments repeated once a week for 28 days (Fig. 5A). Neurological and motor functions were evaluated at multiple time points using a battery of tests, including mNSS, Foot-Fault Test, Rotarod Test, and Cylinder Test. By day 28, the EEVs-treated group exhibited significantly lower mNSS scores compared to the EVs-treated group (Fig. 5B). Starting at day 14, a marked reduction in forelimb foot faults was observed in the EEVs-treated group compared to the EVs-treated group (Fig. 5C). From day 7 onwards, the EEVs-treated group displayed significantly longer latencies to fall in the Rotarod Test (Fig. 5D). Additionally, improved forelimb use symmetry was observed in the EEVs-treated group compared to the EVs-treated group, beginning at day 14 (Fig. 5E).

Although 7T-MRI analysis (Fig. 5F) revealed a reduction in brain lesion volume in EEVs-treated rats compared to PBS-treated rats by day 28 post-injury, this difference did not reach statistical significance. Nevertheless, the observed behavioral improvements collectively indicate that EEVs treatment significantly promotes neuroprotection and neurofunctional recovery following TBI.

EEVs enhance brain plasticity and neurogenesis after TBI

We further explored the mechanisms by which EEVs promote neurofunctional recovery post-TBI. Consistent with the observed behavioral improvements, TBI rats treated with EEVs exhibited significant increases in dendritic spine density, neuronal branching, and total dendritic length by day 28 post-injury compared to the PBS and EVs groups (Fig. 6A-D). Specifically, EEVs-treated group showed a higher number of neuronal branches per neuron and dendritic spines, as well as a marked elongation of total dendritic length, indicating enhanced synaptic connectivity and neuronal structural integrity.

To further examine EEVs's influence on neuronal proliferation and migration, in vitro scratch assays were performed using HT22 neurons treated with DMSO, PBS, EVs, or EEVs. The results demonstrated that EEVs treatment significantly accelerated scratch closure compared to the other groups (Fig. 6E), suggesting enhanced neuronal migration and regenerative capacity. By 12 h post-scratch, neurons in the EEVs group had migrated more rapidly, filling a greater area of the scratch compared to those in the PBS and EVs groups. These results are consistent with the in vivo findings and collectively suggest that EEVs facilitate brain plasticity and neurogenesis, contributing to improved neurological recovery post-TBI.

EEVs reduce neuronal apoptosis by suppressing neuroinflammation

Next, we sought to determine whether EEVs treatment modulate local inflammatory responses and neuronal apoptosis in the peri-lesional cortex. As shown in Fig. 7A, on day 5 post-injury, EEVs and EVs treatments significantly reduced the expression levels of multiple inflammatory cytokines (IL-1α, IL-1β, IL-6, CCL3, INOS, TNF-α) in the peri-lesional area of TBI rats compared to the PBS group, with EEVs showing superior efficacy over EVs. These findings were further corroborated by ELISA,

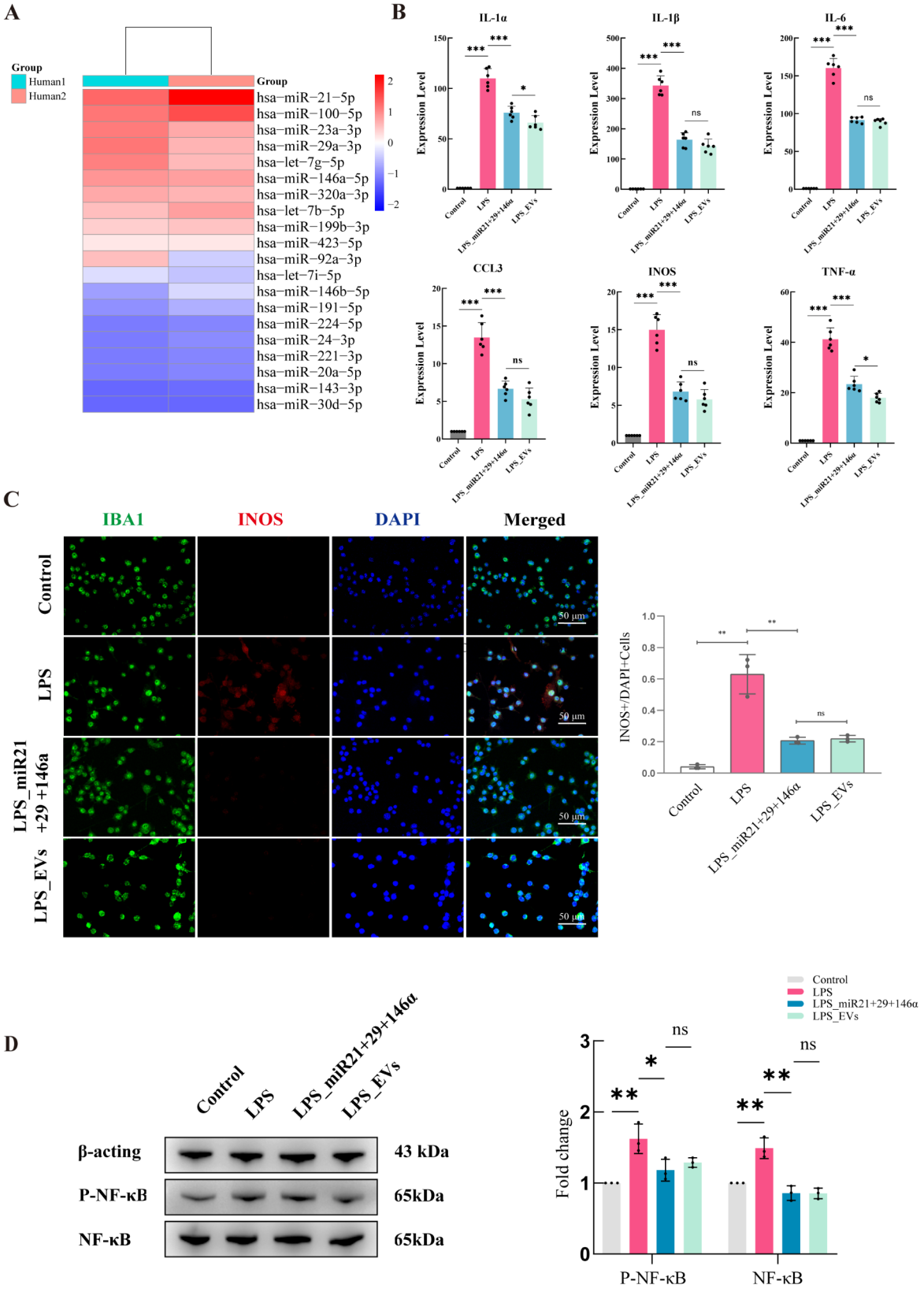

Fig. 3 (See legend on next page.)

(See figure on previous page.)

Fig. 3 Identification of miRNAs in EVs that inhibit microglial activation through the NF-κB signaling pathway. (**A**) Heatmap of miRNA expression levels from high-throughput sequencing of EVs derived from adipose tissue of two human donors, with red indicating high expression and blue indicating low expression. (**B**) qRT-PCR analysis of inflammatory cytokines (IL-1α, IL-1β, IL-6, CCL3, INOS, TNF-α) in an in vitro BV2 microglial activation model ($n=6$). (**C**) IF of IBA1 (green) and INOS (red) in an in vitro BV2 microglial activation model treated with 20 μg total protein of EVs ($n=3$). (**D**) Western blot analysis of NF-κB signaling pathway proteins (P-NF-κB and NF-κB) in the BV2 microglial activation model ($n=3$). *$P<0.05$, **$P<0.01$, ***$P<0.001$

which demonstrated a marked reduction in IL-1β and IL-6 concentrations in the cerebrospinal fluid (CSF) of the EEVs-treated group, underscoring the enhanced anti-inflammatory effects of EEVs(Fig. 7B).

Histopathological analysis using CD68 immunohistochemical staining revealed a significant decrease in the number of CD68-positive microglia in the brain tissues of the EEVs group, indicating lower microglial activation and inflammation. Additionally, NeuN and TUNEL staining demonstrated that EEVs treatment protected neurons by significantly reducing apoptosis. On day 28 post-injury, hematoxylin and eosin (HE) staining was used to assess the integrity of brain tissue. The PBS group exhibited large cavities in the peri-lesional brain tissue, whereas EEVs treatment significantly reduced cavity size, with better outcomes compared to the EVs group (Fig. 7C). Collectively, these results emphasize that EEVs reduces neuronal apoptosis by effectively suppressing TBI-induced neuroinflammation.

Protective effect of EEVs on brain organoids

To further explore the therapeutic potential of EEVs in humans, we generated brain organoids derived from human-induced pluripotent stem cells (hiPSCs) (Fig. 8A). Initially, we characterized the brain organoids using specific markers for neurons (NEUN), microglia (IBA1), and astrocytes (GFAP), confirming the distribution of these cell types within the organoids (Fig. 8B). We then established an LPS-induced inflammation model in the brain organoids and treated them with either EVs or EEVs. The results showed that, compared to the LPS and LPS_EVs groups, the LPS_EEVs group exhibited significantly lower expression levels of inflammatory cytokines, including IL-1α, IL-1β, IL-6, CCL3, INOS, and TNF-α (Fig. 8C). IF analysis further revealed that INOS expression, which was markedly elevated following LPS treatment, was significantly reduced in the EEVs-treated group (Fig. 8D). These findings indicate that EEVs exerts a stronger anti-inflammatory effect, effectively mitigating neuroinflammation in brain organoids.

Discussion

In this study, we developed EEVs that combine intranasal administration with magnetic targeting to efficiently deliver miRNAs specifically targeting the NF-κB signaling pathway to the brain. Our findings demonstrate that these EEVs effectively accumulate at the injury site, suppress neuroinflammation, enhance neuroplasticity, and significantly improve neurological function following TBI. Furthermore, the EEVs exhibited a robust protective effect against inflammatory damage in human brain organoids.

Neuroinflammation is recognized as a critical driver of secondary injury mechanisms in TBI, exacerbating brain tissue damage through a complex cascade of inflammatory responses. This cascade leads to excitotoxicity, oxidative stress, BBB disruption, and neuronal cell death [38]. The amplification of these inflammatory responses not only directly causes neuronal damage and death but also induces apoptosis and tissue fibrosis, further impairing neurological function [39]. Microglia, the resident immune cells of the CNS, play a pivotal role in the pathophysiology of TBI. Upon injury, microglia are the first responders within the CNS, rapidly transforming into an activated state with amoeboid morphology, exhibiting phagocytic activity, and releasing inflammatory mediators [40]. Increasing evidence supports the efficacy of therapeutic strategies aimed at targeting microglial activation to suppress neuroinflammation [41, 42]. For instance, Ekdahl et al. found that brain inflammation significantly inhibits the survival of newly generated hippocampal neurons through microglial activation, while the use of minocycline to inhibit microglial activation could restore neurogenesis under inflammatory conditions [43]. Similarly, Monje et al. demonstrated that indomethacin could restore neurogenesis following endotoxin-induced inflammation [44].

EVs possess natural advantages such as low immunogenicity, good biocompatibility, and stability, making them ideal carriers for delivering therapeutic molecules like proteins, RNA, and small-molecule drugs [45]. However, EVs generally exhibit low bioavailability in vivo, especially when administered systemically. They are often cleared by the host immune system or distributed to non-target tissues before reaching the intended site, which diminishes their therapeutic efficacy [46]. Additionally, the inherent targeting specificity of EVs is limited, making it challenging to ensure their effective accumulation at disease sites, which compromises their clinical utility [47].

To address these limitations, EEVs technologies have been developed. These technologies can significantly enhance the cargo-loading capacity of EVs and improve their targeting to specific injured areas [48].

In the context of neurological diseases, EVs carrying miRNAs have shown significant therapeutic potential by regulating gene expression in target cells. This has been

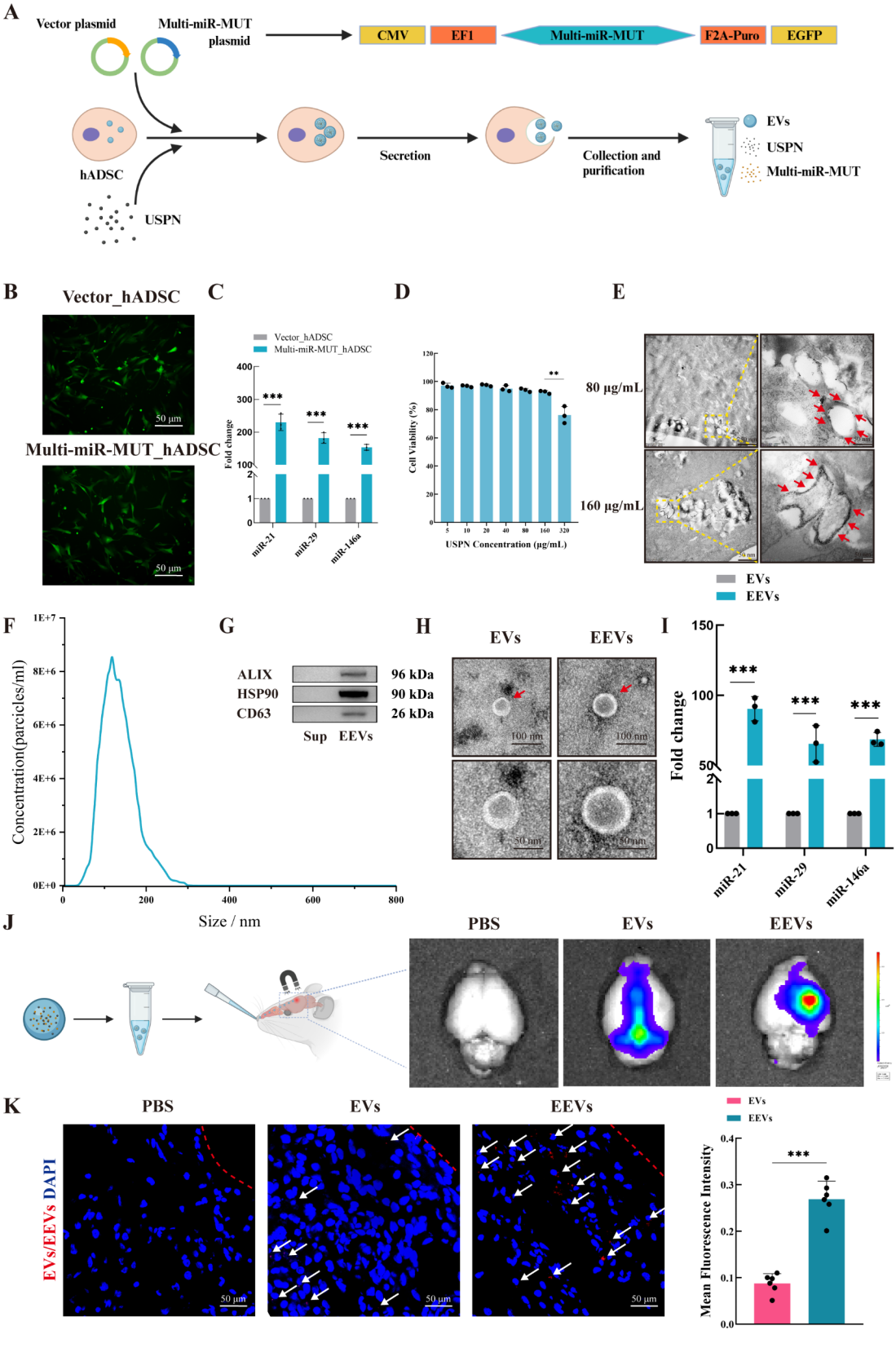

Fig. 4 (See legend on next page.)

(See figure on previous page.)

Fig. 4 Construction of EEVs targeting the injury site. (**A**) Schematic diagram of the EEVs construction process. (**B**) IF showing successful transfection of hADSCs with Multi-miR-MUT and vector lentivirus, indicated by green fluorescence. (**C**) qRT-PCR analysis of hsa-miR-21-5p, hsa-miR-29a-3p, and hsa-miR-146a-5p expression levels in hADSCs after transfection with Multi-miR-MUT and vector lentivirus ($n=3$). **D**) CCK8 assay results showing the effect of different USPN concentrations on hADSC viability ($n=3$). (**E**) TEM showing intracellular accumulation levels of USPN at different concentrations in hADSCs. Red arrows indicate the localization of USPN within the cells. (**F**) NTA analysis confirming the size distribution of EEVs. (**G**) Western blot analysis of characteristic extracellular vesicle proteins in EEVs. (**H**) TEM of EV and EEVs. Red arrows indicate the EV and EEVs structures in the image. (**I**) qRT-PCR analysis of hsa-miR-21-5p, hsa-miR-29a-3p, and hsa-miR-146a-5p expression levels in EEVs and EVs ($n=3$). (**J**) Schematic of in vivo tracking of EVs + DiI and EEVs + DiI after intranasal administration. Red fluorescence indicates the localization of DiI-labeled EVs and EEVs in the brain. Excitation wavelength of 553 nm and emission wavelength of 570 nm. (**K**) IF analysis showing the distribution of PBS, EVs + DiI, and EEVs + DiI in brain sections. Red fluorescence (arrows) represents the presence of DiI-labeled EVs and EEVs in the peri-lesional area ($n=6$). $^{*}P<0.05$, $^{**}P<0.01$, $^{***}P<0.001$. CCK8: Cell Counting Kit-8; ALIX: ALG-2-Interacting Protein X; HSP90: Heat Shock Protein 90; CD63: Cluster of Differentiation 63; Sup: Supernatant; NTA: Nanoparticle tracking analysis; TEM: Transmission electron microscopy

particularly evident in disease models such as Alzheimer's disease, Parkinson's disease, and ischemic stroke [49, 50]. In our study, hsa-miR-21-5p, hsa-miR-29a-3p, and hsa-miR-146a-5p were identified as key regulators capable of inhibiting microglial activation, which is crucial for mitigating neuroinflammation.

miR-21-5p has demonstrated significant biological functions, particularly in inflammation inhibition and tissue repair. Liu et al. found that miR-21-5p from adipose-derived stem cell (ADSC)-derived EVs promotes the polarization of microglia to the M2 phenotype, thereby reducing neuroinflammation following cerebral ischemia [51]. Additionally, He et al. showed that encapsulating human umbilical mesenchymal stem cell (HUMSC)-derived EVs in polyvinyl alcohol (PVA) hydrogel (EVs@PVA) enhances the ability of miR-21-5p to promote osteogenic differentiation of bone marrow stem cells (BMSCs) by inhibiting WWP1-mediated KLF5 ubiquitination and to enhance angiogenesis in human umbilical vein endothelial cells (HUVECs) by targeting ATP2B4 [52].

hsa-miR-29a-3p plays a significant role in regulating cell differentiation and inflammation. It has been shown to enhance tendon repair by targeting PTEN and activating the mTOR/TGF-β1 signaling pathway [53]. Du et al. also demonstrated that miR-29a-3p inhibits Th1 cell differentiation by targeting T-bet, reducing inflammation in a collagen-induced arthritis (CIA) mouse model, a mechanism that may be relevant in other neuroinflammatory diseases [54].

hsa-miR-146a-5p is widely recognized as a negative regulator of neuroinflammation. It promotes the polarization of macrophages from the M1 to M2 phenotype by inhibiting TRAF6 expression, which enhances endothelial cell proliferation, migration, and angiogenesis—mechanisms that accelerate the healing of diabetic wounds and offer new therapeutic strategies for refractory diabetic wounds [55]. Liu et al. found that miR-146a-5p significantly promotes cardiomyocyte proliferation and inhibits apoptosis by negatively regulating its target gene MYBL1, thereby reducing inflammatory responses [56].

We demonstrated that EVssomal hsa-miR-21-5p, hsa-miR-29a-3p, and hsa-miR-146a-5p effectively inhibit the activation of NF-κB signaling pathway, thereby suppressing the production of pro-inflammatory cytokines. The NF-κB signaling pathway plays a critical regulatory role in inflammatory responses within the CNS and has been extensively studied as a key target in neuroinflammation and neurodegenerative diseases [34–36]. Under normal conditions, NF-κB is sequestered in the cytoplasm in an inactive form by binding to inhibitory κB (IκB) proteins [57]. Upon degradation of IκB, NF-κB rapidly translocates to the nucleus, where it recognizes and binds to NF-κB response elements in regulatory gene regions, leading to the transcriptional activation of inflammatory mediators such as IL-6, TNF-α, and COX2. This pathway is one of the most crucial in the pathology mediated by neuroinflammation [58]. Blocking the NF-κB signaling pathway has been shown to significantly reduce neuroinflammation and improve neurofunctional recovery [59, 60].

Intranasal drug delivery is a non-invasive method for administering therapeutics directly to the CNS through the nasal cavity, bypassing the BBB and avoiding first-pass hepatic metabolism. This approach offers higher drug bioavailability and reduces systemic side effects [33]. The mechanisms by which drugs reach the CNS via the nasal route primarily involve the olfactory and trigeminal nerve pathways [61]. The olfactory nerve pathway is one of the key routes, where drugs traverse the nasal mucosa into the brain through both intracellular and extracellular transport mechanisms [62]. Intracellular transport includes small molecules entering olfactory neurons via receptor-mediated endocytosis, eventually being transported along axons to the olfactory bulb and released into postsynaptic cells [63]. Extracellular transport, on the other hand, involves the movement of drugs through the fluid surrounding neurons, directly reaching the CNS [64]. The convenience and safety of intranasal delivery make it a powerful tool for treating neurological diseases, particularly in situations requiring rapid and direct drug delivery to the brain, such as in cases of neuroinflammation and Alzheimer's disease [65–67].

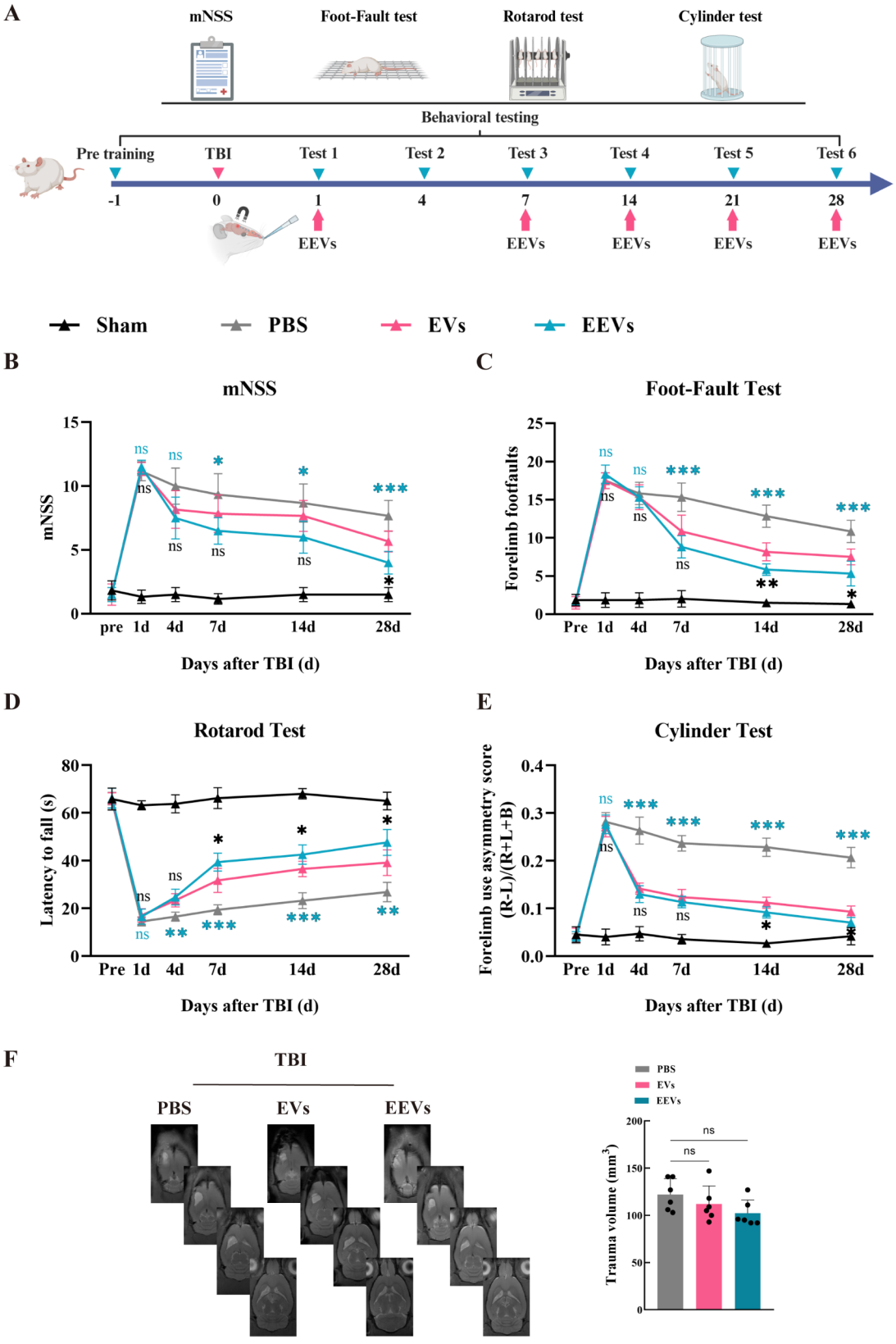

Fig. 5 (See legend on next page.)

(See figure on previous page.)

Fig. 5 EEVs enhance neurofunctional recovery in TBI rats after intranasal administration. (**A**) Schematic representation of the experimental timeline for neurofunctional and behavioral assessments after intranasal administration of EEVs. Neurological and motor function recovery at various time points post-injury was evaluated using the mNSS (**B**), Foot-Fault Test (**C**), Rotarod Test (**D**), and Cylinder Test (**E**) ($n = 6$). (**F**) Evaluation of lesion volume in TBI rats at 28 days post-injury using 7T-MRI ($n = 6$). Statistical analysis was performed using two-way repeated measures ANOVA followed by the Holm-Sidak post hoc multiple comparison test. Color Coding and Statistical Comparisons: Black (EEVs vs. EVs). Blue (EEVs vs. PBS). $^{*}P < 0.05$, $^{**}P < 0.01$, $^{***}P < 0.001$

In this study, we successfully integrated ultra-small superparamagnetic nanoparticles into EVs, enabling precise targeting to brain injury sites through external magnetic field control. This approach significantly enhanced the EVs targeting ability, allowing for more effective accumulation at the injury site and improving therapeutic efficacy. Similarly, Wang et al. developed EVs encapsulating iron oxide nanoparticles (IONPs) and β-lapachone (Lapa), utilizing magnetic guidance to enhance endocytosis in ovarian cancer cells. The Lapa generated H2O2 selectively and depleted intracellular GSH, enhancing oxidative stress and exerting anti-tumor effects [68]. Li et al. demonstrated that a therapeutic platform based on EEVs conjugated with magnetic nanoparticles improved drug targeting and ferroptosis in glioblastoma [69].

To further validate the effectiveness of EEVs in humans, we conducted in-depth studies using human brain organoid models. We found that EEVs significantly reduced neuroinflammatory responses in these organoids. In related research, Lai et al. generated human cortical organoids via hiPSC induction and simulated TBI using high-intensity focused ultrasound, discovering that targeted inhibition of KCNJ2 reduced acute neuronal death and alleviated neurodegenerative processes in the human cortical organoids [70].

Limitations and future perspectives

Despite demonstrating the therapeutic potential of EEVs in the treatment of TBI, this study has several notable limitations. First, the small sample size in behavioral experiments may increase the risk of false-positive results. Although a randomized trial design was employed, multicenter studies are necessary to control for potential evaluation biases. Second, while magnetic targeting showed promise in enhancing EVs delivery, its safety and long-term efficacy in clinical applications require further investigation. Additionally, the distribution accuracy of magnetically targeted EVs may be influenced by the complex magnetic environment within the body, necessitating evaluation in larger and more complex animal models.

In conclusion, while this study reveals the substantial potential of EEVs for treating neurological disorders, significant challenges remain for clinical translation. Future research should focus on optimizing the technology, expanding its application scope, and validating its effectiveness and safety through clinical trials to facilitate the clinical adoption of this emerging therapeutic approach, ultimately providing new hope for patients with neurological diseases.

Materials and methods

Cell culture

Human adipose tissue was obtained following protocols approved by the Ethics Committee of Peking Union Medical College and the Chinese Academy of Medical Sciences. hADSCs were isolated from adipose tissue of healthy volunteers and cultured as described previously [71]. Cells were passaged every two days, and passages 4–5 were used for all experiments. Additional cell lines included BV2 mouse microglial cells (Procell, CL-0493), HT22 mouse hippocampal neuronal cells (Procell, CL-0697), and hiPSC human induced pluripotent stem cells (Shownin, RC01001). All cultures were tested for mycoplasma contamination. BV2 and HT22 cells were maintained in DMEM/F12 (Gibco, 11330032) supplemented with 10% fetal bovine serum (FBS) (Gibco, A5670701), 1% penicillin-streptomycin (Yensen, 60162ES76). hiPSCs were cultured in ncTarget hPSC Medium (Shownin, RP01020). All cells were incubated at 37 °C in a humidified atmosphere containing 5% CO2.

EVs isolation and characterization

EVs were isolated as previously described [72]. When hADSCs reached 70–80% confluence, cells were washed three times with phosphate-buffered saline (PBS) (Gibco, 10010500) and cultured in serum-free medium for 36 h. The supernatant was collected and centrifuged at 3000 rpm for 30 min at room temperature to remove dead cells. The supernatant was then filtered through a 0.22 μm vacuum filter (Corning, 30758) to eliminate large vesicles and cellular debris. The filtrate was transferred to a 100 kDa ultrafiltration tube (Merck, UFC910096), centrifuged at 4 °C, and washed twice with PBS. The EVs retained on the filter membrane were collected and filtered through a 0.2 μm filter (Pall, 4612). The samples were aliquoted into 1.5 mL sterile EP tubes and stored at -80 °C.

For TEM observation, EVs were fixed with 2.5% glutaraldehyde at 4 °C overnight. After thorough washing, the EV suspension was loaded onto Copper mesh and allowed to adsorb for 20 min. Excess liquid was carefully removed with filter paper. The grids were then negatively stained with 2% phosphotungstic acid (pH 7.0) for 60 s, air-dried, and imaged using a TEM-1400plus (Japan) at an acceleration voltage of 80 kV. Particle size and

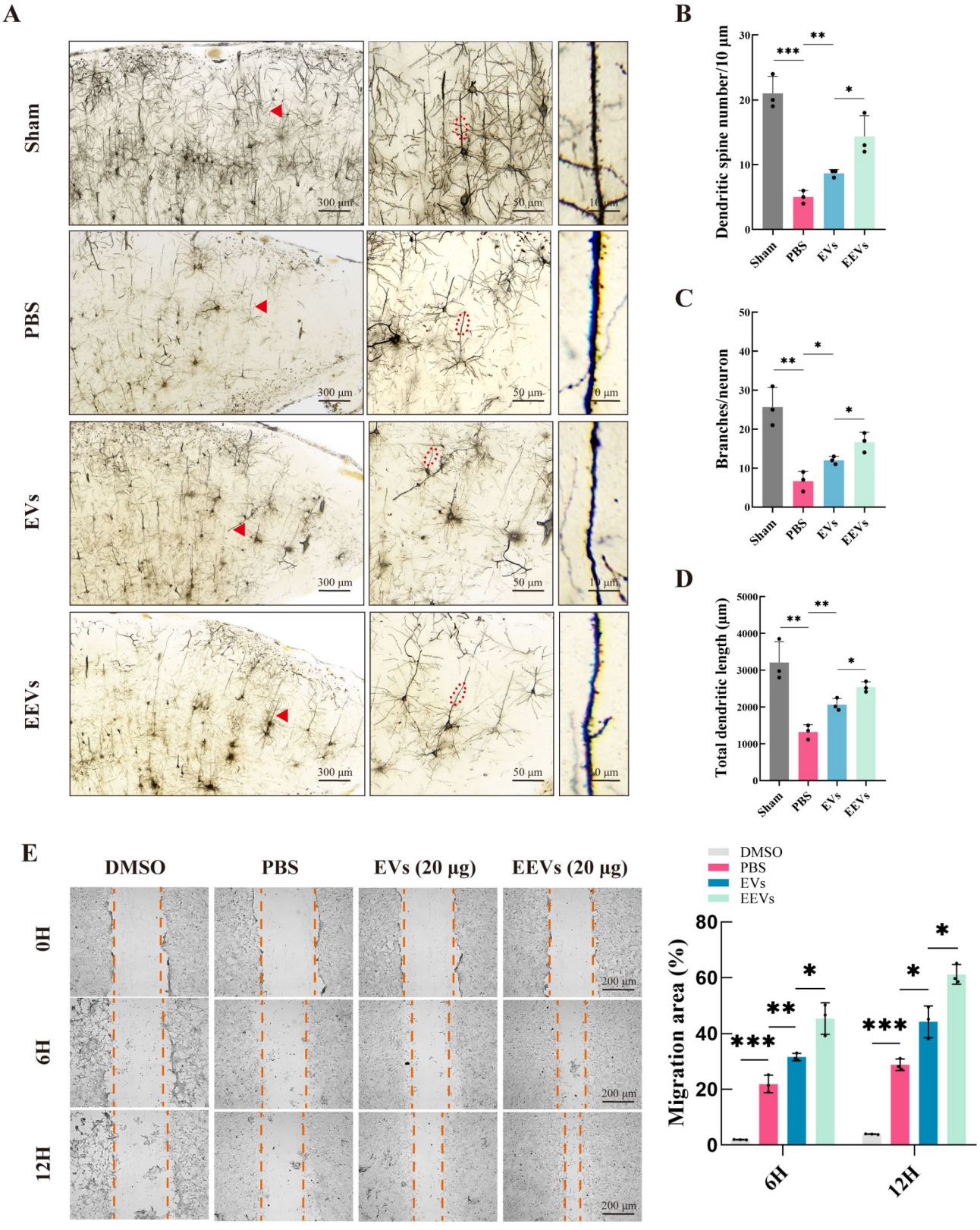

Fig. 6 EEVs promotes brain plasticity and neurogenesis after TBI. (**A**) Golgi-Cox staining of cortical neurons in the perilesional area on day 28 post-injury, with Sholl analysis used to assess dendritic spines (**B**), branching (**C**), and length (**D**) across different intervention groups ($n=3$). (**E**) In vitro neuronal scratch assay showing differences between intervention groups ($n=3$). *$P<0.05$, **$P<0.01$, ***$P<0.001$. DMSO: Dimethyl Sulfoxide

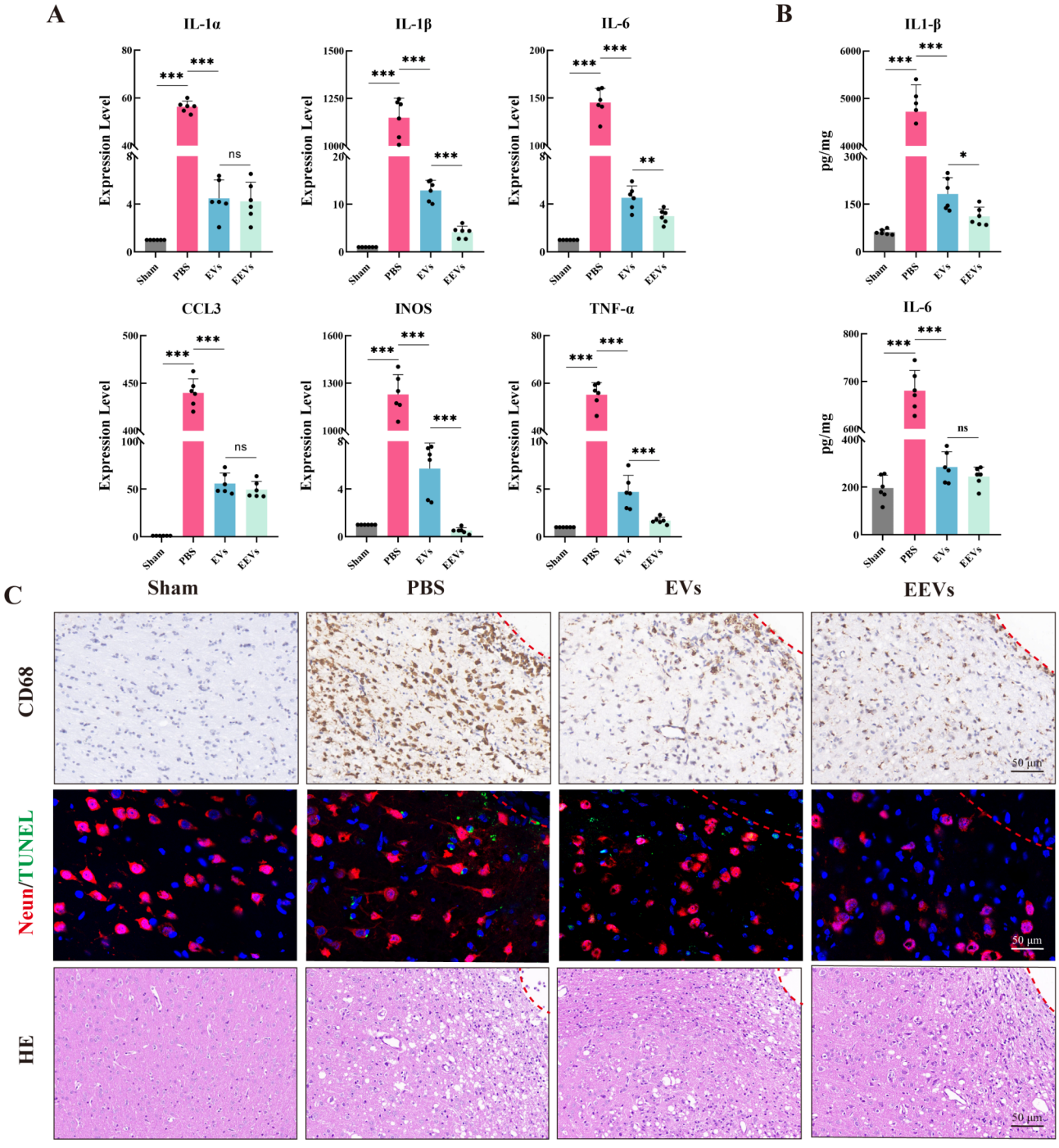

Fig. 7 EEVs reduces neuronal apoptosis by inhibiting neuroinflammation. (**A**) qRT-PCR analysis of inflammatory cytokine expression levels (IL-1α, IL-1β, IL-6, CCL3, INOS, TNF-α) in perilesional brain tissue on day 5 post-TBI ($n=6$). (**B**) ELISA analysis of inflammatory cytokine concentrations (IL-1β, IL-6) in CSF on day 5 post-TBI ($n=6$). (**C**) Immunohistochemistry showing CD68 expression levels in perilesional brain tissue on day 5 post-TBI. IF showing TUNEL staining and NeuN in perilesional brain tissue on day 5 post-TBI. HE staining showing the integrity of perilesional brain tissue on day 28 post-TBI ($n=3$). *$P<0.05$, **$P<0.01$, ***$P<0.001$. TUNEL: Terminal deoxynucleotidyl transferase dUTP nick-end labeling; HE: Hematoxylin-eosin staining; CSF: Cerebrospinal fluid; CD68: Cluster of Differentiation 68

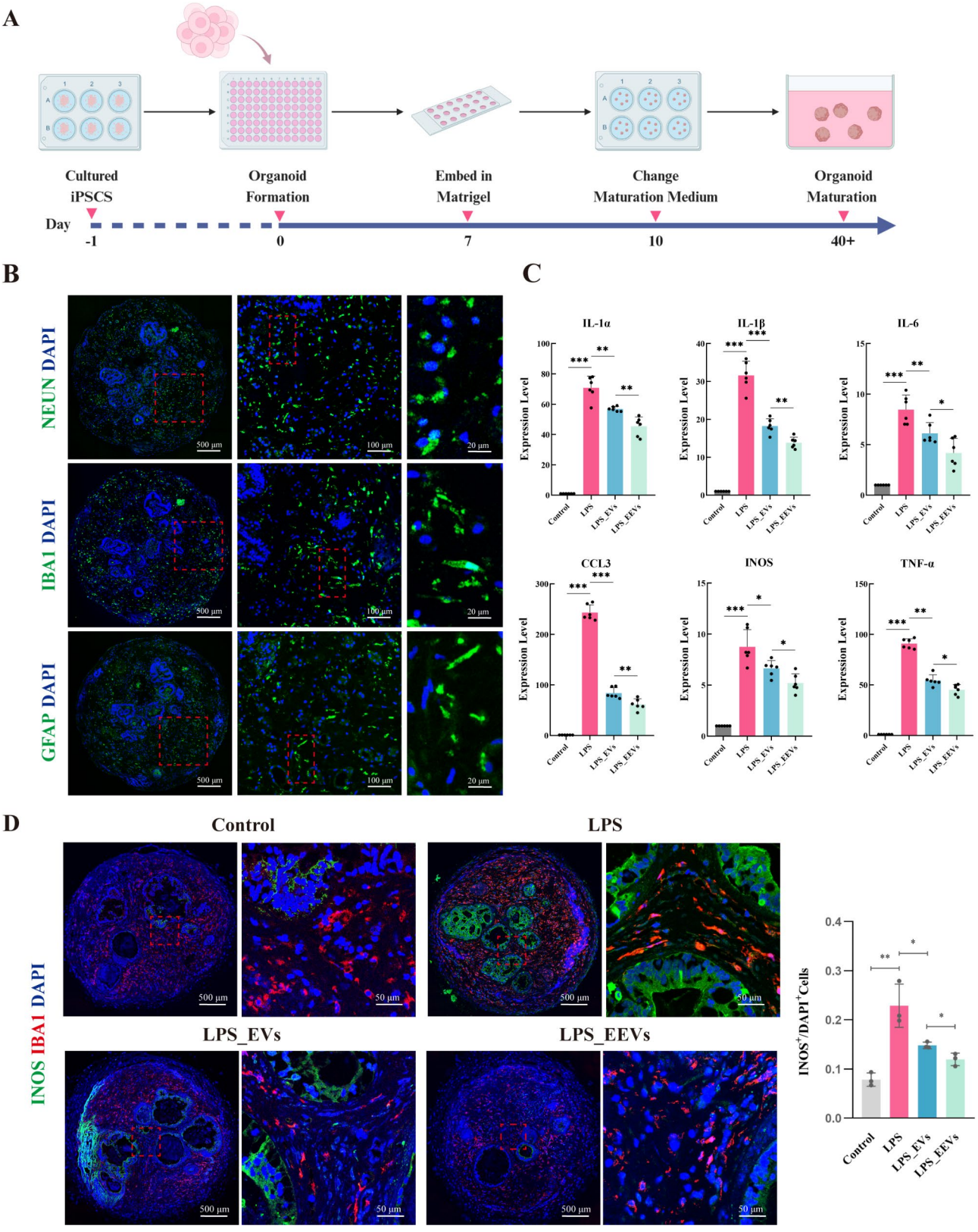

Fig. 8 (See legend on next page.)

(See figure on previous page.)

Fig. 8 Protective effect of EEVs on human brain organoids. (**A**) Schematic diagram of the process of inducing mature human brain organoids from hiPSCs. (**B**) IF showing the distribution of neurons (NeuN), microglia (IBA1), and astrocytes (GFAP) in mature human brain organoids. (**C**) qRT-PCR analysis of inflammatory cytokine expression levels (IL-1α, IL-1β, IL-6, CCL3, INOS, TNF-α) in the inflammation model of human brain organoids ($n = 6$). (**D**) IF showing IBA1 (red) and INOS (green) expression in the inflammation model of human brain organoids treated with 20 μg total protein of EVs/EEVs ($n = 3$). *$P < 0.05$, **$P < 0.01$, ***$P < 0.001$. hiPSCs: human-induced pluripotent stem cells

concentration were determined by Flow NanoAnalysis (Nanofcm, China). The expression of EVs marker proteins was confirmed by Western blotting.

Animal experiments and behavioral assessments

Adult male SD rats (Charles River, China), aged 6 to 8 weeks and weighing 300 ± 11 g, were housed in the animal facility of Peking Union Medical College Hospital under controlled temperature and humidity conditions with a 12-hour light-dark cycle in specific pathogen-free (SPF) conditions. A traumatic brain injury (TBI) model was established using the Feeney free-fall method by dropping a 25 g weight from a height of 20 cm onto the rat's brain [73]. Neurological severity was assessed 24 h post-TBI using mNSS, and only rats with scores ranging between 7 and 12 were selected for inclusion in the study to ensure a consistent model of moderate injury. Animals were randomly assigned to groups.

Intranasal administration was performed as previously described [74]. Briefly, 30 min before administration, the nasal passages were cleared with hyaluronidase (100 U/5 μL per nostril) (Mackin, H810948). Subsequently, 20 μL of EVs/EEVs (20 μg total protein, 2.0×10^{10} particles/mL), hADSCs (5.0×10^5 cells per rat), or PBS was intranasally administered to each nostril using a micropipette with a 10 μL pipette tip [18, 75]. The animals were then placed in a supine position for 10 minutes. This procedure was conducted as a continuous intranasal administration once a week for 28 days, totaling four administrations per animal.

To evaluate the effects of EVs/EEVs/hADSCs/PBS on neurological deficits after TBI, two blinded investigators conducted behavioral assessments using the mNSS, Foot-Fault Test, Rotarod Test, and Cylinder Test on days 1, 4, 7, 14, 21, and 28 post-injury [18, 76, 77].

Multi-miR-MUT transfection in hADSCs

hADSCs were transduced with Multi-miR-MUT (obtained from OBiO Technology, China) at 30–40% confluency during passages 2–3. Cells were infected with lentiviral vectors constructed with Multi-miR-MUT (pcSLenti-EF1-EGFP-F2A-Puro-CMV-pri-hsa-miR-21(mut 3p)-pri-hsa-miR-29a(mut 5p)-pri-hsa-miR-146a(mut 5p)-WPRE) or the corresponding empty vector (pcSLenti-EF1-EGFP-F2A-Puro-CMV-MCS-WPRE) at a multiplicity of infection (MOI) of 20. The transduced cells were incubated at 37 °C with 5% CO2 for 8 h, after which the medium was replaced with fresh medium. Cells were then incubated for an additional 24 h before further analysis.

USPN internalization in hADSCs

USPN (2–3 nm) were obtained from LABKS (JK-01-025). To assess the cytotoxicity of USPNs on hADSCs, various concentrations (5, 10, 20, 40, 80, 160, and 320 μg/mL) were added to the culture medium after the cells had adhered. Cell viability was measured 24 h later using the CCK-8 assay. To evaluate the internalization of USPNs by hADSCs, the cells were treated with 80 and 160 μg/mL concentrations of USPNs for 24 h, followed by visualization using TEM. Based on the results of the CCK-8 assay and TEM, a concentration of 160 μg/mL USPNs was used for subsequent experiments.

EVs miRNA high-throughput sequencing

EVs miRNA sequencing was conducted following the standard protocol provided by Illumina. Library preparation and sequencing were performed using the TruSeq Small RNA Sample Prep Kits (Illumina, USA). The libraries were sequenced on an Illumina Hiseq 2000/2500 platform, generating single-end 50 bp (SE50) reads. Bioinformatic analysis was carried out using ACGT101-miR (v4.2).

Transwell assay

To investigate the regulatory effect of hADSCs on LPS-induced activation of BV2 microglial cells, a Transwell co-culture system (Corning, 3412) was utilized for in vitro experiments. Initially, BV2 cells were seeded in the lower chamber of a 6-well plate at a density of 1×10^5 cells/mL and cultured in DMEM medium supplemented with 10% FBS until they reached 70–80% confluence. BV2 cells were then treated with 100 ng/mL LPS (Sigma-Aldrich, L2880) to induce activation for 6 h, followed by replacing the medium with fresh culture medium. In the upper chamber of the Transwell insert (pore size 0.4 μm), hADSCs were seeded at a density of 1×10^5 cells/mL. The upper and lower chambers allowed indirect communication through soluble factors in the culture medium while preventing direct cell-to-cell contact. hADSCs were cultured in serum-free DMEM to ensure that the regulatory effects in the co-culture system were solely mediated by the secreted factors from hADSCs. After 24 h of co-culture, BV2 cells from the lower chamber were collected for subsequent qRT-PCR analysis and IF.

Immunofluorescence and immunohistochemistry staining

IF and immunohistochemistry were performed as previously described [18]. For IF, cells were permeabilized with Triton X-100 (Beyotime, P0096) for 10 min, followed by blocking with 3% bovine serum albumin (BSA) (Yeasen, 36101ES80) for 1 h. Samples were incubated with primary antibodies overnight at 4 °C, followed by incubation with secondary antibodies at room temperature for 1 h. Slides were mounted with anti-fade mounting medium containing DAPI (Beyotime, P0131). For immunohistochemistry, sections were incubated with primary antibodies overnight at 4 °C, followed by incubation with a biotinylated secondary antibody and subsequently with an avidin-biotin-peroxidase complex. Visualization was achieved using Fast DAB Peroxidase Substrate (Sigma-Aldrich, D0426), followed by hematoxylin counterstaining. Imaging was performed using a Leica Laser Scanning Confocal Microscope (SP8 STED 3X) (Leica, Germany).

Primary antibodies used included NeuN (CST, 24307T, 1:100), GFAP (CST, 80788T, 1:200), IBA1 (CST, 17198T, 1:200), IBA1 (Abcam, 283319, 1:100), CD68 (Abcam, 283654, 1:50), INOS (MedChemExpress, HY-P80725, 1:200), and ARG1 (Proteintech, 16001-1-AP, 1:200). Secondary antibodies used included Goat Anti-Rabbit IgG Alexa Fluor® 488 (Abcam, 150081, 1:500), Goat Anti-Rabbit IgG Alexa Fluor® 647 (CST, 4414S, 1:500), and Goat Anti-Mouse IgG Alexa Fluor® 647 (Abcam, 150119, 1:500).

Quantitative analysis of fluorescence intensity was performed using ImageJ software (version 1.54f). The mean fluorescence intensity (MFI) was measured for each sample. Five randomly selected fields were analyzed per sample, and the values were averaged across three biological replicates for each group.

TUNEL staining for apoptotic neurons

To assess neuronal cell death in TBI rats, TUNEL staining was performed on coronal brain cryosections using a One-Step TUNEL Apoptosis Assay Kit (Green Fluorescence) (Beyotime, C1086) according to the manufacturer's instructions.

In vivo Tracking of EVs

For in vivo tracking of EVs, labeling was conducted using Dil dye (Invitrogen, C7000) or PKH67 Green Fluorescent Cell Linker Kit (Solarbio, D0031) according to the manufacturer's protocol. Briefly, diluted dye was incubated with EVs for 30 min, followed by transfer to a 100 kDa ultrafiltration tube. The mixture was diluted with PBS to 10 mL, centrifuged at 4 °C, and washed twice with PBS to remove excess unbound dye. Fluorescence microscopy was employed to confirm uniform labeling of EVs without aggregation.

PBS, dye-labeled EVs, and dye-labeled EEVs were administered intranasally 24 h post-injury, with a 5 mm external magnet positioned over the injury site. Forty-eight hours after administration, brains were harvested, and fluorescence imaging was performed using the Perkin Elmer IVIS Spectrum In Vivo Imaging System (PerkinElmer, USA). Whole-brain fluorescence images were captured and analyzed using Living Image® 4.5.5 Software (PerkinElmer, USA).

Enzyme-linked immunosorbent assay (ELISA)

On day 5 post-TBI, CSF was collected from the cisterna magna of the rats. IL-1β and IL-6 protein levels in the CSF were quantified by researchers blinded to the experimental groups, following the manufacturer's instructions (Multi Sciences, EK301BHS-96, EK306HS-96).

Western blotting

Protein extraction was performed using RIPA lysis buffer (Applygen, C1053) supplemented with PMSF (Solarbio, P8340). The protein concentration was quantified using a BCA Protein Assay Kit (Beyotime, P0011). Equal amounts of protein were separated by SDS-PAGE and transferred onto PVDF membranes (Millipore, ISEQ00010). The membranes were blocked with 5% non-fat milk in TBST (Tris-buffered saline with 0.1% Tween-20) for 1 h at room temperature and incubated overnight at 4 °C with the following primary antibodies: IBA1 (CST, 17198T), IL-1β (Abcam, 234437), ARG1 (Proteintech, 16001-1-AP), NF-κB (CST, 8242T), Phospho-NF-κB (CST, 3033T), ALIX (Abcam, 275377), Hsp90 (CST, 4874S), and CD63 (Abcam, 134045). After washing, the membranes were incubated with HRP-conjugated secondary antibodies for 1 h at room temperature. Protein bands were visualized using an enhanced chemiluminescence (ECL) detection system. β-actin (CST,4970S) was used as the internal loading control.

Quantitative real-time polymerase chain reaction(qRT-PCR)

Brain tissues or cells were lysed and sonicated using TRIzol (Invitrogen, 10296010). Total RNA was extracted following the manufacturer's instructions and treated with DNase I (Sigma-Aldrich, AMPD1). cDNA was synthesized using a High-Capacity cDNA Reverse Transcription Kit (Takara, RR037Q). qRT-PCR was performed on a StepOnePlus Real-Time PCR System (Bio-Rad) using TB Green Mastermix (Takara, R075A). Relative mRNA expression levels were calculated using the–ΔΔCt method and normalized to GAPDH. Primer sequences are listed in Supplementary Table S1.

Generation of human brain organoids

The generation of human brain organoids was carried out following the instructions provided with the STEMdiff™

Cerebral Organoid Kit (STEMCELL, 08570). Briefly, on Day 0, hiPSCs were cultured in embryoid bodie (EB) Seeding Medium to form EBs. From Day 2 to Day 5, 100 µL of EB Formation Medium was added to each well daily. On Day 5, the EBs were observed, and their diameters were approximately 400–600 µm. From Day 5 to Day 7, the medium was replaced with Induction Medium, and the EBs were expected to grow to a visible size of around 500–800 µm in diameter. From Day 7 to Day 10, the EBs were embedded in Matrigel (Corning, 354277) and further cultured in Expansion Medium. The embedded organoids continued to expand, developing neuroepithelial structures. From Day 10 to Day 40+, the medium was replaced with Maturation Medium, and the organoid plates were placed on an orbital shaker in an incubator at 37 °C for constant shaking. The medium was changed every 3–4 days until the organoids reached maturity around Day 40. Mature organoids reached a diameter of approximately 3–5 mm, with a dense central region and cortical cell distribution.

Statistical analysis

Data were analyzed using GraphPad Prism 8.0 software. Results are presented as mean ± standard deviation (SD). Statistical significance was determined using Student's t-test for comparisons between two groups, or two-way repeated measures ANOVA followed by the Holm-Sidak post hoc test for comparisons involving more than two groups. A significance threshold was set at $^{*}P < 0.05$, $^{**}P < 0.01$, and $^{***}P < 0.001$.

Abbreviations

TBI	Traumatic Brain Injury
CNS	Central Nervous System
BBB	Blood-Brain Barrier
NF-κB	Nuclear Factor kappa B
miRNA	MicroRNA
EVs	Extracellular vesicles
EEVs	Engineered Extracellular vesicles
hADSC	Human Adipose-Derived Stem Cell
MSC	Mesenchymal Stem Cell
IBA1	Ionized Calcium-Binding Adapter Molecule 1
NEUN	Neuronal Nuclei
GFAP	Glial Fibrillary Acidic Protein
IL-1β	Interleukin-1 beta
TNF-α	Tumor Necrosis Factor-alpha
IL-6	Interleukin-6
CCL3	Chemokine (C-C motif) ligand 3
INOS	Inducible Nitric Oxide Synthase
ARG1	Arginase 1
TEM	Transmission Electron Microscopy
WB	Western Blot
NTA	Nanoparticle Tracking Analysis
qRT-PCR	Real-Time Quantitative Polymerase Chain Reaction
USPN	Ultra-Small Paramagnetic Nanoparticles
LPS	Lipopolysaccharide
hiPSC	Human-induced pluripotent stem cells
BDNF	Brain-Derived Neurotrophic Factor
VEGF	Vascular Endothelial Growth Factor
MRI	Magnetic Resonance Imaging
mNSS	Modified Neurological Severity Score
CCK-8	Cell Counting Kit-8
HE	Hematoxylin and Eosin (staining)
TUNEL	Terminal Deoxynucleotidyl Transferase dUTP Nick-End Labeling
ELISA	Enzyme-Linked Immunosorbent Assay
EB	Embryoid Body
PBS	Phosphate-Buffered Saline
PVA	Polyvinyl Alcohol
IONP	Iron Oxide Nanoparticle
GBM	Glioblastoma
HUVEC	Human Umbilical Vein Endothelial Cell
ADSC	Adipose-Derived Stem Cell
DMSO	Dimethyl Sulfoxide

Supplementary Information

The online version contains supplementary material available at https://doi.org/10.1186/s12951-025-03181-9 .

Supplementary Material 1

Acknowledgements

We extend our gratitude to the State Key Laboratory of Research on the Mechanisms of Major Diseases at the Institute of Basic Medical Sciences, Chinese Academy of Medical Sciences, for their invaluable assistance with tissue processing and immunofluorescence staining. We also sincerely appreciate the support from the Laboratory Animal Platform of the National Major Scientific and Technological Infrastructure for Translational Medicine at Peking Union Medical College Hospital, which facilitated the animal experiments. Additionally, some images in this article were created using BioRender.com.

Author contributions

PTL was responsible for the overall methodology, conducting experiments, analyzing data, and drafting and revising the manuscript. JJW, QH, and RCHZ conceived the idea, provided supervision, guidance on experimental planning, and secured funding. JJW was the first corresponding author, provided financial support for the experiments, and oversaw project administration. SSS, XYZ, XYL, RY, YHC assisted with the animal studies, while SSS, JBC, SHW, LGY, JXG, XYZ, HSX, YW, WZ, ZS, XZ contributed to the in vitro cell experiments. All authors contributed to the writing of the manuscript and have read and approve the manuscript.

Funding

This research was supported by the National High Level Hospital Clinical Research Funding (2022-PUMCH-C-032).

Data availability

No datasets were generated or analysed during the current study.

Declarations

Ethical approval

The publication of this article has been approved by all authors.

Consent for publication

Not applicable.

Competing interests

The authors declare no competing interests.

Author details

[1]Department of Neurosurgery, Peking Union Medical College Hospital, Peking Union Medical College, Chinese Academy of Medical Sciences, Beijing, China
[2]School of Basic Medicine, Institute of Basic Medical Sciences Chinese Academy of Medical Sciences, Peking Union Medical College, Beijing, China
[3]Department of Oncology, Peking Union Medical College, Peking Union Medical College Hospital, Chinese Academy of Medical Sciences, Beijing, China

Received: 21 November 2024 / Accepted: 1 February 2025
Published online: 21 March 2025

References

1. Mollayeva T, Mollayeva S, Colantonio A. Traumatic brain injury: sex, gender and intersecting vulnerabilities. Nat Rev Neurol. 2018;14:711–22.
2. Jiang JY, Gao GY, Feng JF, Mao Q, Chen LG, Yang XF, Liu JF, Wang YH, Qiu BH, Huang XJ. Traumatic brain injury in China. Lancet Neurol. 2019;18:286–95.
3. Rauen K, Reichelt L, Probst P, Schäpers B, Müller F, Jahn K, et al. Quality of life up to 10 years after traumatic brain injury: a cross-sectional analysis. Health Qual Life Outcomes. 2020;18(1):166.
4. Yang Y, Li Z, Fan X, Jiang C, Wang J, Rastegar-Kashkooli Y, Wang TJ, Wang J, Wang M, Cheng N, et al. Nanozymes: potential therapies for reactive oxygen species overproduction and inflammation in ischemic stroke and traumatic brain Injury. ACS Nano. 2024;18:16450–67.
5. Chen Y, Long T, Chen J, Wei H, Meng J, Kang M, et al. WTAP participates in neuronal damage by protein translation of NLRP3 in an m6A-YTHDF1-dependent manner after traumatic brain injury. Int J Surg. 2024;110(9):5396–408.
6. Aqel S, Al-Thani N, Haider MZ, Abdelhady S, Al Thani AA, Kobeissy F, et al. Biomaterials in traumatic brain injury: perspectives and challenges. Biology (Basel). 2023;13(1):21.
7. Bacakova L, Zarubova J, Travnickova M, Musilkova J, Pajorova J, Slepicka P, et al. Stem cells: their source, potency and use in regenerative therapies with focus on adipose-derived stem cells - a review. Biotechnol Adv. 2018;36:1111–26.
8. Qin Y, Ge G, Yang P, Wang L, Qiao Y, Pan G, Yang H, Bai J, Cui W, Geng D. An update on adipose-derived stem cells for Regenerative Medicine: where Challenge meets opportunity. Adv Sci (Weinh). 2023;10:e2207334.
9. Kolle SF, Fischer-Nielsen A, Mathiasen AB, Elberg JJ, Oliveri RS, Glovinski PV, Kastrup J, Kirchhoff M, Rasmussen BS, Talman ML, et al. Enrichment of autologous fat grafts with ex-vivo expanded adipose tissue-derived stem cells for graft survival: a randomised placebo-controlled trial. Lancet. 2013;382:1113–20.
10. Moon KC, Suh HS, Kim KB, Han SK, Young KW, Lee JW, Kim MH. Potential of allogeneic adipose-derived stem cell-hydrogel complex for treating Diabetic Foot Ulcers. Diabetes. 2019;68:837–46.
11. Thesleff T, Lehtimaki K, Niskakangas T, Huovinen S, Mannerstrom B, Miettinen S, Seppanen-Kaijansinkko R, Ohman J. Cranioplasty with adipose-derived stem cells, Beta-tricalcium phosphate granules and supporting mesh: six-year clinical Follow-Up results. Stem Cells Transl Med. 2017;6:1576–82.
12. Sarveazad A, Newstead GL, Mirzaei R, Joghataei MT, Bakhtiari M, Babahajian A, Mahjoubi B. A new method for treating fecal incontinence by implanting stem cells derived from human adipose tissue: preliminary findings of a randomized double-blind clinical trial. Stem Cell Res Ther. 2017;8:40.
13. Qayyum AA, Mathiasen AB, Helqvist S, Jorgensen E, Haack-Sorensen M, Ekblond A, Kastrup J. Autologous adipose-derived stromal cell treatment for patients with refractory angina (MyStromalCell Trial): 3-years follow-up results. J Transl Med. 2019;17:360.
14. Courtine G, Sofroniew MV. Spinal cord repair: advances in biology and technology. Nat Med. 2019;25:898–908.
15. Song N, Scholtemeijer M, Shah K. Mesenchymal stem cell immunomodulation: mechanisms and therapeutic potential. Trends Pharmacol Sci. 2020;41:653–64.
16. Giro O, Jimenez A, Pane A, Badimon L, Ortega E, Chiva-Blanch G. Extracellular vesicles in atherothrombosis and cardiovascular disease: friends and foes. Atherosclerosis. 2021;330:61–75.
17. Hong P, Yang H, Wu Y, Li K, Tang Z. The functions and clinical application potential of exosomes derived from adipose mesenchymal stem cells: a comprehensive review. Stem Cell Res Ther. 2019;10:242.
18. Chen Y, Li J, Ma B, Li N, Wang S, Sun Z, Xue C, Han Q, Wei J, Zhao RC. MSC-derived exosomes promote recovery from traumatic brain injury via microglia/macrophages in rat. Aging. 2020;12:18274–96.
19. Aimaletdinov AM, Gomzikova MO. Tracking of extracellular vesicles' biodistribution: new methods and approaches. Int J Mol Sci. 2022;23(19):11312.
20. Toh WS, Zhang B, Lai RC, Lim SK. Immune regulatory targets of mesenchymal stromal cell exosomes/small extracellular vesicles in tissue regeneration. Cytotherapy. 2018;20:1419–26.
21. Xu H, Jia Z, Ma K, Zhang J, Dai C, Yao Z, Deng W, Su J, Wang R, Chen X. Protective effect of BMSCs-derived exosomes mediated by BDNF on TBI via miR-216a-5p. Med Sci Monit. 2020;26:e920855.
22. Zhang H, Wu J, Wu J, Fan Q, Zhou J, Wu J, Liu S, Zang J, Ye J, Xiao M, et al. Exosome-mediated targeted delivery of miR-210 for angiogenic therapy after cerebral ischemia in mice. J Nanobiotechnol. 2019;17:29.
23. Tian T, Zhang HX, He CP, Fan S, Zhu YL, Qi C, Huang NP, Xiao ZD, Lu ZH, Tannous BA, Gao J. Surface functionalized exosomes as targeted drug delivery vehicles for cerebral ischemia therapy. Biomaterials. 2018;150:137–49.
24. Alvarez-Erviti L, Seow Y, Yin H, Betts C, Lakhal S, Wood MJ. Delivery of siRNA to the mouse brain by systemic injection of targeted exosomes. Nat Biotechnol. 2011;29:341–5.
25. Li P, Yin R, Chen Y, Chang J, Yang L, Liu X, Xu H, Zhang X, Wang S, Han Q, Wei J. Engineered extracellular vesicles for ischemic stroke: a systematic review and meta-analysis of preclinical studies. J Nanobiotechnol. 2023;21:396.
26. Shahjin F, Chand S, Yelamanchili SV. Extracellular vesicles as Drug Delivery vehicles to the Central Nervous System. J Neuroimmune Pharmacol. 2020;15:443–58.
27. Lochhead JJ, Thorne RG. Intranasal delivery of biologics to the central nervous system. Adv Drug Deliv Rev. 2012;64:614–28.
28. Aly AE, Waszczak BL. Intranasal gene delivery for treating Parkinson's disease: overcoming the blood-brain barrier. Expert Opin Drug Deliv. 2015;12:1923–41.
29. Betzer O, Perets N, Angel A, Motiei M, Sadan T, Yadid G, Offen D, Popovtzer R. In vivo neuroimaging of Exosomes using gold nanoparticles. ACS Nano. 2017;11:10883–93.
30. Guo S, Perets N, Betzer O, Ben-Shaul S, Sheinin A, Michaelevski I, Popovtzer R, Offen D, Levenberg S. Intranasal delivery of mesenchymal stem cell derived exosomes loaded with phosphatase and tensin homolog siRNA repairs complete spinal cord Injury. ACS Nano. 2019;13:10015–28.
31. Perets N, Betzer O, Shapira R, Brenstein S, Angel A, Sadan T, Ashery U, Popovtzer R, Offen D. Golden exosomes selectively target brain pathologies in neurodegenerative and neurodevelopmental disorders. Nano Lett. 2019;19:3422–31.
32. Cheng YQ, Yue YX, Cao HM, Geng WC, Wang LX, Hu XY, Li HB, Bian Q, Kong XL, Liu JF, et al. Coassembly of hypoxia-sensitive macrocyclic amphiphiles and extracellular vesicles for targeted kidney injury imaging and therapy. J Nanobiotechnol. 2021;19:451.
33. Keller LA, Merkel O, Popp A. Intranasal drug delivery: opportunities and toxicologic challenges during drug development. Drug Deliv Transl Res. 2022;12:735–57.
34. Sivandzade F, Prasad S, Bhalerao A, Cucullo L. NRF2 and NF-κB interplay in cerebrovascular and neurodegenerative disorders: molecular mechanisms and possible therapeutic approaches. Redox Biol. 2019;21:101059.
35. Zhang L, Zhao G, Luo Z, Yu Z, Liu G, Su G, Tang X, Yuan Z, Huang C, Sun HS, et al. AD16 attenuates neuroinflammation induced by cerebral ischemia through down-regulating astrocytes A1 polarization. Biomed Pharmacother. 2024;178:117209.
36. Wahl D, Risen SJ, Osburn SC, Emge T, Sharma S, Gilberto VS, Chatterjee A, Nagpal P, Moreno JA, LaRocca TJ. Nanoligomers targeting NF-kappaB and NLRP3 reduce neuroinflammation and improve cognitive function with aging and tauopathy. J Neuroinflammation. 2024;21:182.
37. Nouri Z, Barfar A, Perseh S, Motasadizadeh H, Maghsoudian S, Fatahi Y, Nouri K, Yektakasmaei MP, Dinarvand R, Atyabi F. Exosomes as therapeutic and drug delivery vehicle for neurodegenerative diseases. J Nanobiotechnol. 2024;22:463.
38. Simon DW, McGeachy MJ, Bayir H, Clark RS, Loane DJ, Kochanek PM. The far-reaching scope of neuroinflammation after traumatic brain injury. Nat Rev Neurol. 2017;13:171–91.
39. Zhong W, Li T, Hou S, Zhang H, Li Z, Wang G, Liu Q, Song X. Unsupervised disentanglement strategy for mitigating artifact in photoacoustic tomography under extremely sparse view. Photoacoustics. 2024;38:100613.
40. Donat CK, Scott G, Gentleman SM, Sastre M. Microglial activation in traumatic brain Injury. Front Aging Neurosci. 2017;9:208.
41. Qi Z, Peng J, Wang H, Wang L, Su Y, Ding L, Cao B, Zhao Y, Xing Q, Yang JJ. Modulating neuroinflammation and cognitive function in postoperative cognitive dysfunction via CCR5-GPCRs-Ras-MAPK pathway targeting with microglial EVs. CNS Neurosci Ther. 2024;30:e14924.
42. Chae S, Lee HJ, Lee HE, Kim J, Jeong YJ, Lin Y, Kim HY, Leriche G, Ehrlich RS, Lingl SC, et al. The dopamine analogue CA140 alleviates AD pathology, neuroinflammation, and rescues synaptic/cognitive functions by modulating DRD1 signaling or directly binding to Abeta. J Neuroinflammation. 2024;21:200.

43. Ekdahl CT, Claasen JH, Bonde S, Kokaia Z, Lindvall O. Inflammation is detrimental for neurogenesis in adult brain. Proc Natl Acad Sci U S A. 2003;100:13632–7.
44. Monje ML, Toda H, Palmer TD. Inflammatory blockade restores adult hippocampal neurogenesis. Science. 2003;302:1760–5.
45. Herrmann IK, Wood MJA, Fuhrmann G. Extracellular vesicles as a next-generation drug delivery platform. Nat Nanotechnol. 2021;16:748–59.
46. Hilt AJ. Evolving Roles of Health Care Organizations in Community Development. AMA J Ethics. 2019;21:E201–206.
47. Xu M, Feng T, Liu B, Qiu F, Xu Y, Zhao Y, Zheng Y. Engineered exosomes: desirable target-tracking characteristics for cerebrovascular and neurodegenerative disease therapies. Theranostics. 2021;11:8926–44.
48. Wang J, Wang M, Jiang N, Ding S, Peng Q, Zheng L. Emerging chemical engineering of exosomes as bioscaffolds in diagnostics and therapeutics. Genes Dis. 2023;10:1494–512.
49. Parhizkar A, Asgary S. Local Drug Delivery Systems for Vital Pulp Therapy: A New Hope. *Int J Biomater* 2021, 2021:5584268.
50. Bezzini DR, Washington GN, Abiodun O, Olufajo OA, Jones I, Butts DM, Ortega G, Paul H. The potential impact of plastic surgery expertise on Body Contouring Procedure outcomes. Aesthet Surg J. 2021;41:47–55.
51. Liu C, Yin T, Zhang M, Li Z, Xu B, Lv H, Wang P, Wang J, Hao J, Zhang L. Function of mir-21-5p derived from ADSCs-exos on the neuroinflammation after cerebral ischemia. J Stroke Cerebrovasc Dis. 2024;33:107779.
52. He L, Zhang H, Zhao N, Liao L. A novel approach in biomedical engineering: the use of polyvinyl alcohol hydrogel encapsulating human umbilical cord mesenchymal stem cell-derived exosomes for enhanced osteogenic differentiation and angiogenesis in bone regeneration. Int J Biol Macromol. 2024;270:132116.
53. Yao Z, Li J, Xiong H, Cui H, Ning J, Wang S, Ouyang X, Qian Y, Fan C. MicroRNA engineered umbilical cord stem cell-derived exosomes direct tendon regeneration by mTOR signaling. J Nanobiotechnol. 2021;19:169.
54. Du ZH, Chu WX, Peng X, Wu LL, Liu Y, Yu GY, et al. SHED-Derived exosomes ameliorate sjögren's syndrome-induced hyposalivation by suppressing th1 cell response via the miR-29a-3p/T-bet axis. ACS Appl Mater Interfaces. 2025;17(4):5752–61.
55. Zhou X, Ye C, Jiang L, Zhu X, Zhou F, Xia M, Chen Y. The bone mesenchymal stem cell-derived exosomal miR-146a-5p promotes diabetic wound healing in mice via macrophage M1/M2 polarization. Mol Cell Endocrinol. 2024;579:112089.
56. Liu C, Xue J, Xu B, Zhang A, Qin L, Liu J, et al. Exosomes derived from miR-146a-5p-Enriched mesenchymal stem cells protect the cardiomyocytes and myocardial tissues in the polymicrobial sepsis through regulating MYBL1. Stem Cells Int. 2021;1530445.
57. Yamamoto Y, Gaynor RB. IkappaB kinases: key regulators of the NF-kappaB pathway. Trends Biochem Sci. 2004;29:72–9.
58. Tang Y, Le W. Differential roles of M1 and M2 microglia in neurodegenerative diseases. Mol Neurobiol. 2016;53:1181–94.
59. Poonasri M, Mankhong S, Chiranthanut N, Srisook K. 4-methoxycinnamyl p-coumarate reduces neuroinflammation by blocking NF-kappaB, MAPK, and Akt/GSK-3beta pathways and enhancing Nrf2/HO-1 signaling cascade in microglial cells. Biomed Pharmacother. 2023;168:115808.
60. Zhou X, Zhu Y, Gao D, Li M, Lin L, Wang Z, Du H, Xu Y, Liu J, He Y, et al. Matrilin-3 supports neuroprotection in ischemic stroke by suppressing astrocyte-mediated neuroinflammation. Cell Rep. 2024;43:113980.
61. Crowe TP, Greenlee MHW, Kanthasamy AG, Hsu WH. Mechanism of intranasal drug delivery directly to the brain. Life Sci. 2018;195:44–52.
62. Ball MJ, Lukiw WJ, Kammerman EM, Hill JM. Intracerebral propagation of Alzheimer's disease: strengthening evidence of a herpes simplex virus etiology. Alzheimers Dement. 2013;9:169–75.
63. Steinke A, Meier-Stiegen S, Drenckhahn D, Asan E. Molecular composition of tight and adherens junctions in the rat olfactory epithelium and fila. Histochem Cell Biol. 2008;130:339–61.
64. Wu H, Hu K, Jiang X. From nose to brain: understanding transport capacity and transport rate of drugs. Expert Opin Drug Deliv. 2008;5:1159–68.
65. Sood S, Jain K, Gowthamarajan K. Intranasal therapeutic strategies for management of Alzheimer's disease. J Drug Target. 2014;22:279–94.
66. Dutta D, Jana M, Paidi RK, Majumder M, Raha S, Dasarathy S, et al. Tau fibrils induce glial inflammation and neuropathology via TLR2 in Alzheimer's disease-related mouse models. J Clin Invest. 2023;133(18):e161987.
67. Zhong XL, Huang Y, Du Y, He LZ, Chen YW, Cheng Y, Liu H. Unlocking the therapeutic potential of Exosomes Derived from nasal olfactory mucosal mesenchymal stem cells: restoring synaptic plasticity, neurogenesis, and Neuroinflammation in Schizophrenia. Schizophr Bull. 2024;50:600–14.
68. Wang S, Mao Y, Rong S, Liu G, Cao Y, Yang Z, Yu H, Zhang X, Fang H, Cai Z, et al. Engineering magnetic extracellular vesicles mimetics for enhanced targeting chemodynamic therapy to overcome Ovary Cancer. ACS Appl Mater Interfaces. 2024;16:39021–34.
69. Li B, Chen X, Qiu W, Zhao R, Duan J, Zhang S, Pan Z, Zhao S, Guo Q, Qi Y, et al. Synchronous disintegration of Ferroptosis Defense Axis via Engineered Exosome-Conjugated magnetic nanoparticles for Glioblastoma Therapy. Adv Sci (Weinh). 2022;9:e2105451.
70. Lai JD, Berlind JE, Fricklas G, Lie C, Urenda JP, Lam K, Sta Maria N, Jacobs R, Yu V, Zhao Z, Ichida JK. KCNJ2 inhibition mitigates mechanical injury in a human brain organoid model of traumatic brain injury. Cell Stem Cell. 2024;31:519–e536518.
71. Cao Y, Sun Z, Liao L, Meng Y, Han Q, Zhao RC. Human adipose tissue-derived stem cells differentiate into endothelial cells in vitro and improve postnatal neovascularization in vivo. Biochem Biophys Res Commun. 2005;332:370–9.
72. You T, Tang H, Wu W, Gao J, Li X, Li N, Xu X, Xing J, Ge H, Xiao Y, et al. POSTN Secretion by Extracellular Matrix Cancer-Associated fibroblasts (eCAFs) correlates with poor ICB response via Macrophage Chemotaxis activation of akt signaling pathway in gastric Cancer. Aging Dis. 2023;14:2177–92.
73. Feeney DM, Boyeson MG, Linn RT, Murray HM, Dail WG. Responses to cortical injury: I. Methodology and local effects of contusions in the rat. Brain Res. 1981;211:67–77.
74. Ikeda T, Kawabori M, Zheng Y, Yamaguchi S, Gotoh S, Nakahara Y, et al. Intranasal administration of mesenchymal stem cell-derived exosome alleviates hypoxic-ischemic brain injury. Pharmaceutics. 2024;16(4):446.
75. Wang Z, Wang Y, Wang Z, Gutkind JS, Wang Z, Wang F, Lu J, Niu G, Teng G, Chen X. Engineered mesenchymal stem cells with enhanced tropism and paracrine secretion of cytokines and growth factors to treat traumatic brain injury. Stem Cells. 2015;33:456–67.
76. Chen J, Sanberg PR, Li Y, Wang L, Lu M, Willing AE, Sanchez-Ramos J, Chopp M. Intravenous administration of human umbilical cord blood reduces behavioral deficits after stroke in rats. Stroke. 2001;32:2682–8.
77. Yang L, Han B, Zhang Z, Wang S, Bai Y, Zhang Y, Tang Y, Du L, Xu L, Wu F, et al. Extracellular vesicle-mediated delivery of circular RNA SCMH1 promotes functional recovery in Rodent and Nonhuman Primate Ischemic Stroke models. Circulation. 2020;142:556–74.

Publisher's note